PERSPECTIVE

Check for updates

Semi-transparent solar cells: strategies for maximum power output in cities†

Vox Kalai Wong, [a] Johnny Ka Wai Ho, [a] Wallace W. H. Wong [b] and Shu Kong So *[a]

Semi-transparent photovoltaics (STPVs) are a promising form of building-integrated photovoltaics for urban green energy generation. By modulating visible light absorption, STPVs can exhibit both high power conversion efficiency (PCE) and average visible transmittance (AVT). While the maximum PCE for an opaque cell is 33%, the maximum PCE for a highly transparent STPV (70% AVT) has been reported as ~24% by Lunt in 2012. We found that the maximum PCE for STPVs with the same transparency can actually exceed this limit, reaching 28% through band selective (BS) absorption of certain visible wavelengths. This BS method also increases the maximum light utilization efficiency (LUE) from 20% to 23%. Besides performance limits, studying harvestable irradiance for STPVs in urban environments is essential for accurate power output predictions, yet such analyses are rarely found. We analysed solar irradiance in 16 cities over a decade, deriving empirical spectra for both sunny and cloudy conditions. The maximum harvestable irradiance for completely transparent PVs in cities deviates from the AM 1.5G standard (~570 W/m²), yielding ~460 W/m² under clear skies and ~50 W/m² under overcast conditions, with infrared (IR) accounting for 85–90% of invisible irradiance. The corresponding maximum output power intensity ranges from 150 to 250 W/m² (sunny), depending on the absorber's transparency. Our findings reveal that organic materials with IR bandgaps (0.9–1.4 eV) and high AVT are ideal for high-performance STPVs. Examining functional layers shows that some charge extraction layers and encapsulants can impair PCE by blocking invisible light, while metal electrodes could restrict overall transparency unless nanopatterned or thinned. These results offer comprehensive guidance for material scientists and energy researchers in optimizing and analysing STPVs.

Broader context

Cities house about 50% of the global population yet contribute over 70% of CO_2 emissions. Reducing these emissions is crucial, with solar energy playing a vital role. Many cities now implement building integrated photovoltaics (BIPVs). However, traditional solar panels require significant space, making semi-transparent solar cells (STPVs) increasingly attractive. These panels let some visible light to pass through while generating energy. Emerging technologies, such as organic and perovskite solar cells, allow these panels to selectively absorb portions of visible light, either at specific percentages or wavelengths. Here, we assess the solar energy potential of STPVs in urban areas. We identify effective strategies to achieve both high efficiency and transparency by analyzing the maximum performance of various STPV techniques and predicting their power output in cities. We also offer guidance on selecting charge extraction layers, electrodes, and encapsulants by assessing their impact on performance and transparency.

1. Introduction

According to the International Energy Agency, buildings account for 30% of worldwide final energy consumption and 26% of global energy-related carbon emissions. Zero-carbon-ready buildings, which often rely on renewable energy, are vital to mitigate climate change.[1] Solar energy stands out as one of the most accessible green energy options for urban buildings. However, the development of retrofit rooftop solar panels is constrained by rooftop space

a Department of Physics and Institute of Advanced Materials, Hong Kong Baptist University, Hong Kong Special Administrative Region, China.
E-mail: skso@hkbu.edu.hk
b ARC Centre of Excellence in Exciton Science, School of Chemistry, The University of Melbourne, Parkville, Victoria 3010, Australia
† Electronic supplementary information (ESI) available. See DOI: https://doi.org/10.1039/d4ee03757j

This journal is © The Royal Society of Chemistry 2025

Energy Environ. Sci., 2025, **18**, 579–601 | **579**

limitations and aesthetic concerns. Building integrated photovoltaics (BIPVs) have emerged as a solution that seamlessly integrate solar power generation into a building's structure, such as windows and facades. This approach allows for power generation while achieving effective land-use and architectural aesthetics.[2–4] The increasing popularity of windows or semi-transparent envelopes as prominent design elements in modern buildings, such as high-end residential complexes and contemporary shopping malls, has generated significant interest in semi-transparent photovoltaics (STPVs).[4–6]

Researchers have employed various techniques to achieve semi-transparency in single-junction PVs at the device level. As shown in Fig. 1(a), these techniques can be broadly classified
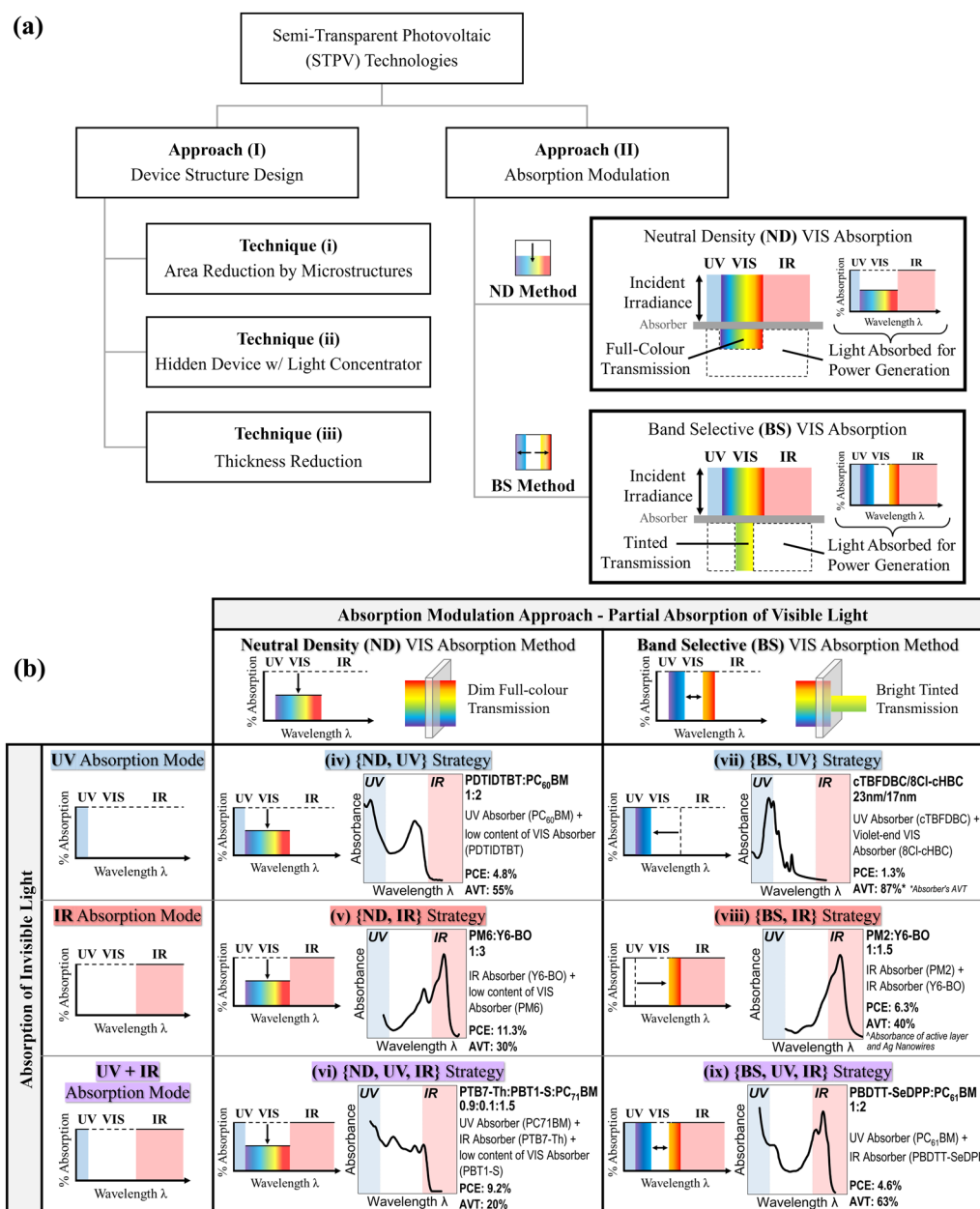
Fig. 1 (a) An overview of STPV technologies, classified into two approaches. Approach (I) involves deliberate device structure design to alleviate VIS blockage, while Approach (II) focuses on regulating light absorption through various VIS and INVIS absorption strategies. In Approach (II), two methods are employed for VIS absorption: neutral density (ND) and band selective (BS). (b) The absorption of INVIS can be grouped into three modes: (iv & vii) UV, (v & viii) IR, and (vi & ix) dual (UV + IR) as depicted in the left panel. By harnessing both INVIS and a portion of VIS for power generation, it is possible to achieve six combinations (iv–ix). Specific examples of STOPV are extracted from relevant literature: (iv),[7] (v),[8] (vi),[9] (vii),[10] (viii),[11] and (ix).[12] In each example, the absorption spectrum of the active layer(s) is presented, with the contribution of each material to the overall absorption characteristics. Additionally, the PCE and AVT of the device are provided for reference.

into two primary approaches: (I) reducing the obstruction of visible light (VIS) through a tactical device configuration, and (II) modulating the absorption of VIS and invisible light (INVIS) *via* materials engineering.

1.1 Approach (I): device structure design

At the device structure level, several techniques are available for achieving semi-transparency. They include (i) minimizing the absorptive area of the device by incorporating micro-structures,[13,14] (ii) utilizing concentrators to direct light to edge-mounted PVs,[15,16] and (iii) significantly reducing the thickness of the entire device.[17,18] An average visible transmittance (AVT) of 20–50% was attained through introducing micro-hole arrays with diameters ranging from 500 nm to 100 μm into initially dark crystalline silicon solar cells.[19] A large-area STPV system was demonstrated using a luminescent solar concentrator to guide light towards stripe PV modules mounted on the edge.[20] The ideal thickness for an opaque perovskite solar cell is typically around 300–500 nm.[21] By reducing the absorber thickness to below 100 nm, originally opaque perovskite solar cells can achieve semi-transparency.[22] While thinning the active layer in many cases does not result in equal absorption attenuation across all wavelengths, it often leads to a weakening of the absorption of both VIS and INVIS.[22–24] Subsequently, there is a linear trade-off between maximum power conversion efficiency (max. PCE) and AVT as given by Lunt's Shockley–Queisser (SQ) limit calculations.[25,26]

1.2 Approach (II): absorption modulation

The strategies for realizing semi-transparency at the materials level involve constraining the absorption of VIS while preferentially absorbing the INVIS for power generation. This strategy holds the potential to sustain a respectable PCE at a high AVT, given that INVIS constitutes over 50% of the solar irradiance. This approach has been generalized by Lunt's UV/NIR wavelength-selective SQ limits, which gives a max. PCE of 20.6% for completely transparent PVs.[25,26] These SQ values are suitable for STPVs that constrain the VIS absorption at a relatively neutral density (ND) to minimize the impact on chromaticity. In Fig. 1(a) within the ND method box under Approach (II), the left illustration depicts an absorber using the ND method. As incident light passes through, it uniformly attenuates the VIS of each colour, resulting in full-colour transmission with reduced irradiance. The right illustration shows the absorbed light, with complete INVIS absorption and partial absorption of VIS at the same percentage for all colours. This method has been mainly adopted in semi-transparent organic solar cells (STOPVs) through adjusting the donor, acceptor or ternary component proportions in the bulk-heterojunction (BHJ) films.[7–9,27,28] In principle, it can also be implemented in layer-by-layer (LBL) STOPVs or other STPVs by stacking a thin layer of a VIS absorber and a thicker INVIS absorber. Nonetheless, there is another method to restrict the VIS absorption in the active layer that is not governed by the existing SQ limits. Semi-transparency can likewise be achieved by absorbing violet-end and/or red-end VIS *via* bandgap engineering of
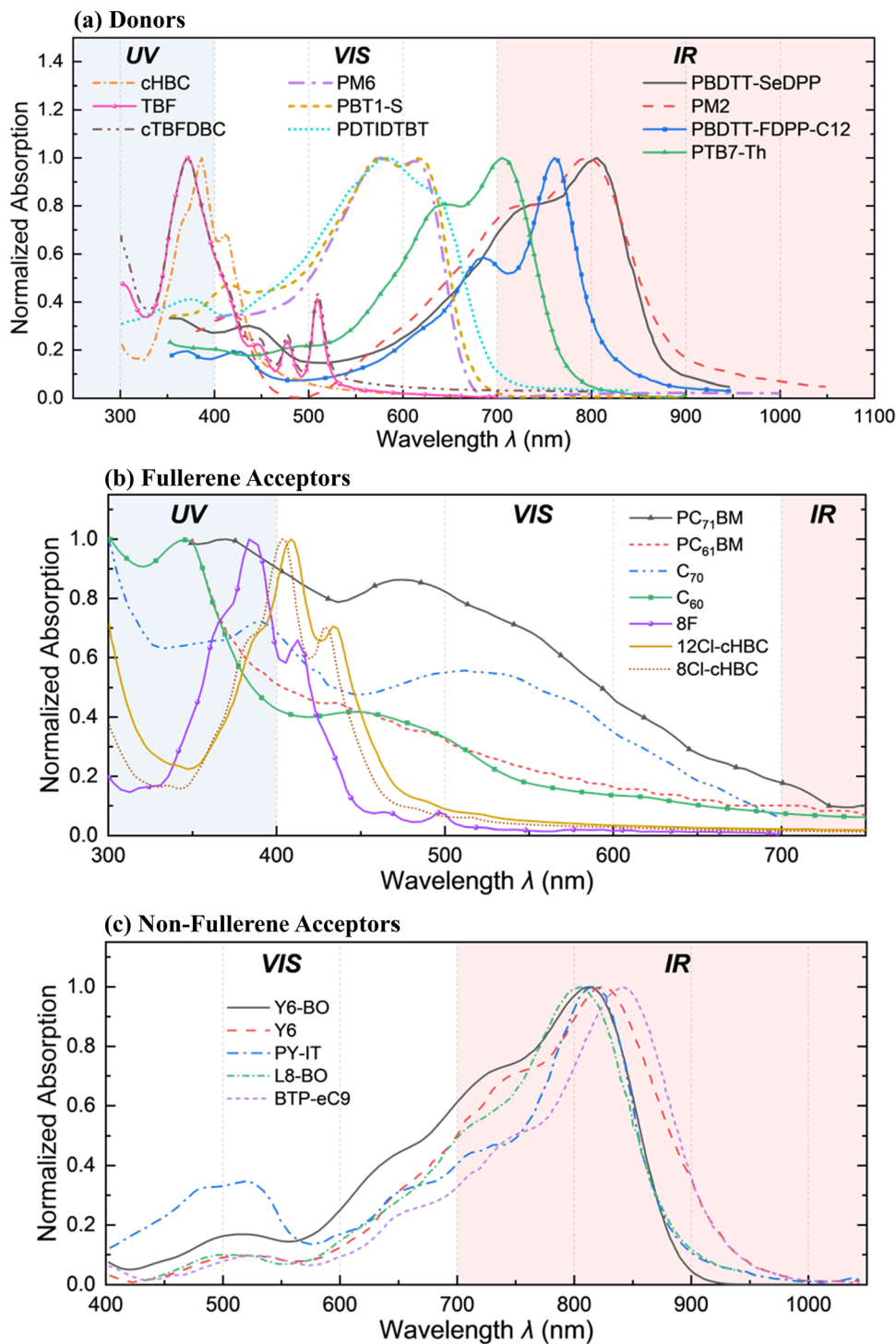
the absorber(s)—referred to as the band selective (BS) VIS absorption method in this work. When employing the BS method, as illustrated in Fig. 1(a) under Approach (II), the absorber selectively captures violet, indigo, blue, orange and red from the incident VIS, while allowing green and yellow to transmit at full intensity. This method results in tinted transmission, with certain colours passing through at their original brightness while others are blocked. In addition to its prevalent use in STOPVs,[10–12,29,30] this method has gained popularity in semi-transparent perovskite photovoltaics (STPPVs),[31–35] enabled by raising the bandgaps to absorb violet VIS and UV lights. Apart from the broader applicability across emerging thin-film photovoltaic technologies, this BS method has theoretical potential for achieving higher efficiency by mitigating thermalization losses from high-energy photons above the bandgap. Yet, the detailed SQ limits for this BS method remain unreported.

As for power generation using INVIS, it can be further segmented into three absorption modes: (1) UV, (2) IR, or (3) dual (UV + IR). Combining the two VIS absorption methods (ND or BS) with the three INVIS absorption modes yields a total of six STPV absorption modulation strategies as shown in Fig. 1(b). Organic materials can be designed to enable strong, narrow absorption in the IR region while maintaining high transmittance in VIS and UV ranges due to electron localization and discrete, narrow-band electronic states with high primary transition rates.[36] This property offers high flexibility in absorption fine-tuning, facilitating the implementation of diverse absorption modulation strategies. The examples used in this work are therefore primarily organic materials. Nevertheless, the findings regarding the harvestable irradiance and SQ limits apply broadly to all STPV systems.

1.3 Implementation of absorption modulation strategies using organic materials

In Fig. 1(b), one STOPV example is provided for each absorption modulation strategy, highlighting their composition, absorption spectrum of the active layer(s), and performance characteristics of the device. In the column for the ND VIS absorption method, researchers can pair UV-absorbing and/or IR-absorbing components with a low concentration of the VIS absorber. If the absorbers are carefully engineered, this method can facilitate neutral VIS transmission and thereby a high colour rendering index (CRI). A notable instance is the ternary STOPV reported by Xie *et al.*, which employs strategy (vi) {ND, UV, IR}. In this device, a fullerene acceptor is utilized as the UV absorber, PTB7-Th as the IR-absorbing polymer donor, and a small dose of PBT1-S as the VIS-absorbing donor to modulate the absorption of VIS. An AVT of 20% was achieved, with CIE colour coordinates of (0.2976, 0.3283) located in close proximity to the standard solar irradiance spectrum AM 1.5G (0.3136, 0.3300), demonstrating high colour fidelity.[9] Meanwhile, BS absorption strategies can be accomplished by combining UV and violet VIS absorbers; and/or IR and red VIS absorbers. This permits high transmission of VIS at specific wavelengths, resulting in tinted films. Utilizing strategy (ix) {BS, UV, IR},

This journal is © The Royal Society of Chemistry 2025

Energy Environ. Sci., 2025, **18**, 579–601 | 581

(a) Donors

(b) Fullerene Acceptors

(c) Non-Fullerene Acceptors

Fig. 2 The absorption spectra of various organic materials used in STPVs, highlighting the UV, VIS, and IR regions. The materials are categorized into three groups: (a) donors, (b) fullerene acceptors, and (c) non-fullerene acceptors. The absorption data presented are obtained from multiple sources.[7–12,40,41]

Chen *et al.* fabricated a green STOPV with a high AVT of 63%.[12] The green colour is a result of a high bandgap fullerene acceptor that absorbs UV and some violet VIS, and a polymer donor PBDTT-SeDPP that absorbs IR and some red VIS, allowing the green VIS to be transmitted.

Fig. 2 shows the absorption spectra of organic materials commonly used in STOPVs, categorized into (a) donors, (b) fullerene acceptors and (c) non-fullerene acceptors.[37] Many of these materials exhibit a distinct and narrow absorption peak within specific wavelength ranges, such as

582 | *Energy Environ. Sci.*, 2025, **18**, 579–601

This journal is © The Royal Society of Chemistry 2025

UV, VIS, or IR regions. The wide choice of materials allows mixing and matching them to reach the desired semi-transparency.[38,39] Regarding donors, UV-absorbing organic materials are often small molecules, whereas IR-absorbing donors tend to be polymers. For the acceptor materials, fullerene acceptors are typically UV or violet VIS absorbers, while non-fullerene acceptors are predominantly IR and red VIS absorbers.

1.4 Contributions of this work

This work aims to provide insights for materials scientists in the field of STPVs through a comprehensive comparison of these six absorption modulation strategies in terms of their maximum power output (P_{out}) when deployed as BIPVs in urban settings. To accomplish this objective, two key inputs were required: an assessment of the harvestable solar irradiance for STPVs in urban environments, as well as the corresponding SQ efficiency limits. Hence, the key contributions of this study are:

(1) To address the fact that solar irradiance in cities can deviate significantly from the standard AM 1.5G spectrum,[42] we conducted an extensive statistical analysis of the solar irradiance data in 16 diverse urban locations around the world under both clear sky and cloudy conditions. This was done to quantify the range of real-world irradiance levels that can impact the performance of STPVs for urban applications.

(2) We then simulated and compared the AVT dependent SQ limits, including the max. PCEs, light utilization efficiencies (LUEs), the ideal bandgap ($E_{g,opt}$), and thus the highest P_{out}, for each of the six STPV absorption modulation strategies (Fig. 1(b)) under both the AM 1.5G spectrum and the empirical urban irradiance identified in the statistical analysis.

(3) We provided an overview of how functional layers other than the active layer can impact the device's PCE and AVT. Specifically, we analysed the optical transmittance of common non-metal charge extraction layers, metal electrodes, and device encapsulants across both INVIS and VIS wavelength ranges. This analysis provides guidance on selecting functional layers to maximize the device's PCE and AVT.

2. Methods

2.1 Statistical analysis of irradiance data

This study examined solar irradiance data from 16 cities, including Vancouver, New York, São Paulo, Berlin, Stockholm, Cairo, Johannesburg, Dubai, Riyadh, Mumbai, Beijing, Hong Kong, Singapore, Tokyo, Melbourne, and Sydney. These cities were chosen to represent a diverse range of geographical locations and climates (as shown in Fig. 3(a)). The data were acquired from the National Aeronautics and Space Administration (NASA) Langley Research Centre (LaRC) Prediction of Worldwide Energy Resource (POWER) Project funded through the NASA Earth Science/Applied Science Program. The dataset utilized in this study is CERES SYN1deg Ed4A, which calculates

surface insolation values based on observations from satellites. These values underwent validation through ground-based measurements carried out by the Baseline Surface Radiation Network (BSRN).[43–45] Each data point is the average hourly solar irradiance at a specific coordinate on Earth. The source data cover the hourly average solar irradiance for every hour and every day between 2013 and 2022. To focus on sensible daytime values, the data for nighttime, as well as the hours of sunrise and sunset, were filtered out.

The average monthly maximum irradiance of the 16 cities over a 10-year period was segmented into three wavelength ranges: ultraviolet (UV, 280–400 nm), visible (VIS, 400–700 nm), and shortwave infrared (IR, 700–3000 nm). These segments were then compared to the AM 1.5G spectrum, resulting in realization rates as depicted in Fig. 3(b). The AM 1.5G spectrum, with a total irradiance of 1000 W/m^2, was developed based on the average atmospheric conditions in the 48 contiguous U.S. states, located in the mid-latitude region of the Northen Hemisphere.[46,47] Notably, the realization rate of UV can exceed 100% because UV exposure is higher in low-latitude and Southern Hemisphere cities due to ozone layer fluctuation,[48] lower zenith angles and prevalent sunny weather patterns typical of tropical or subtropical climates. An estimated spectrum was generated for the average monthly maximum irradiance of the 16 cities by adjusting the AM 1.5G spectrum based on the realization rate for each wavelength range (monthly max. spectrum in Fig. 3(c)). The contribution of each wavelength range to the total solar irradiance in the specific spectrum is summarized in Fig. 3(d).

A similar approach was employed to obtain the cloudy avg. spectrum in Fig. 3(c). In this case, the numerator used for calculating the realization rate was the average solar irradiance during heavily overcast skies (<20% clearness) in the 16 cities over a decade (Fig. 3(b)). The clearness is derived from the ratio of ground-based irradiance to top-of-atmosphere irradiance.[42] Cloud cover is categorized into four groups based on clearness: <20% cloudy, 20–40% mostly cloudy, 40–60% mostly sunny, and > 60% sunny. The maximum clearness index reaches approximately 80%, accounting for around 20% attenuation from the atmosphere, even under cloudless sky conditions.

Both resulting spectra, monthly max. and cloudy avg., alongside the AM 1.5G standard spectrum, are used in the calculation of harvestable irradiance and the SQ limits.

2.2 Harvestable irradiance spectrum and the Shockley–Queisser efficiency limit model

In STPV, a portion of light from the solar spectrum (AM 1.5G, monthly max. or cloudy avg.) is designed to pass through the photovoltaic device. The rest, if not reflected, are absorbed by the device (refer to Fig. 1(a)). The spectrum of the absorbed light is the harvestable irradiance spectrum as shown in Fig. 6. During energy harnessing, only the light absorbed by the STPV device is relevant to its performance; the transmitted light does not interact with the device nor contribute to the performance. Therefore, the Shockley–Queisser (SQ)-limit device parameters
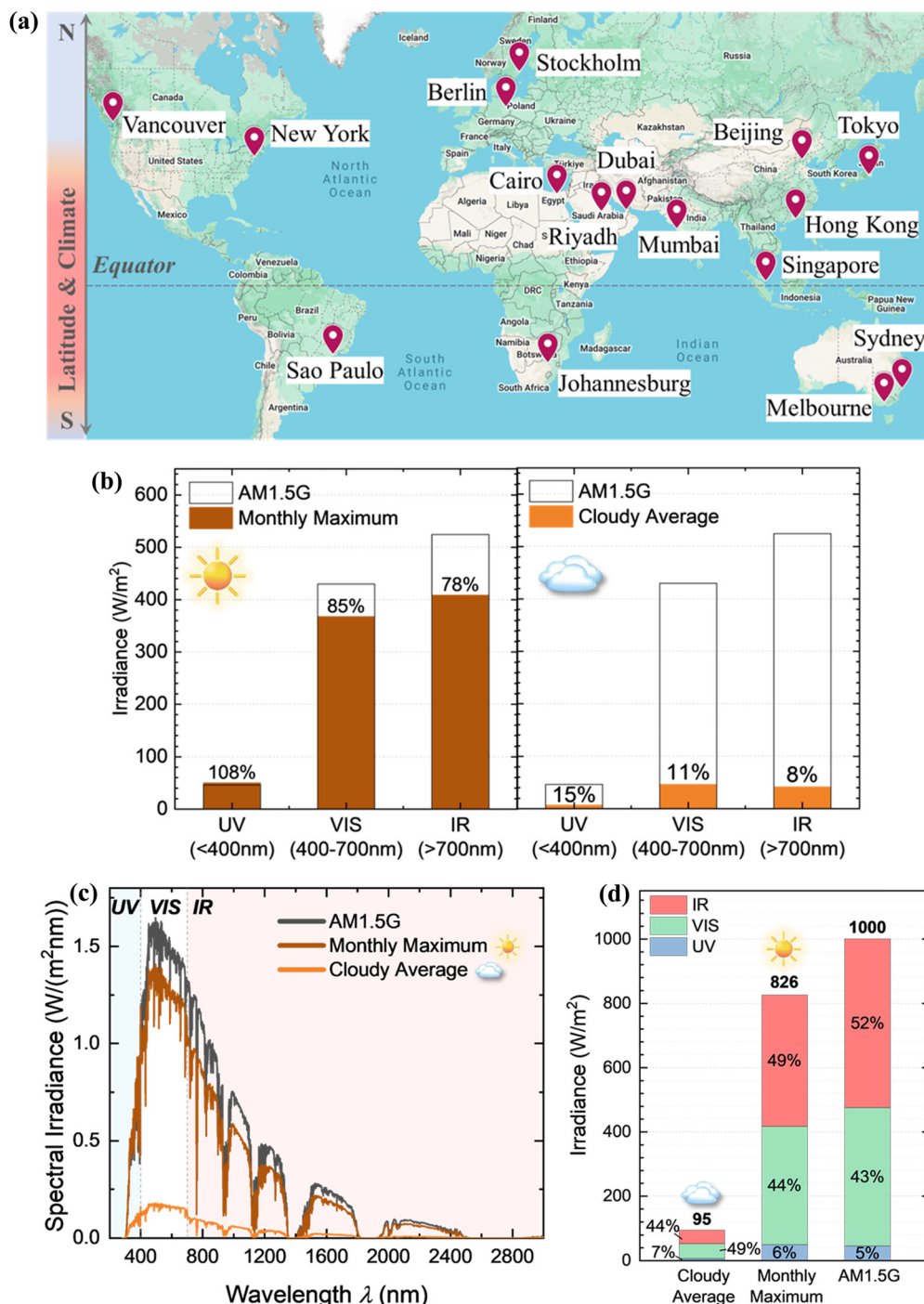
This journal is © The Royal Society of Chemistry 2025

Energy Environ. Sci., 2025, **18**, 579–601 | **583**

Fig. 3 (a) A world map featuring the 16 analysed cities with pins, showing their diverse geographic locations and climates. (b) The realization rates of three wavelength ranges for the average monthly maximum irradiance (left) and the average irradiance during overcast skies (<20% clearness) (right) as compared to the AM 1.5G standard irradiance. (c) The comparison of the standard AM 1.5G spectrum with the estimated monthly max. spectrum and cloudy avg. spectrum, obtained by adjusting the AM 1.5G spectrum based on the corresponding realization rates. (d) The irradiance of each wavelength range and their respective contribution to the total irradiance in various spectra.

of an STPV device can be evaluated by modelling an absorber under the incidence of the *harvestable irradiance spectrum* subject to a specific strategy (ND or BS method and UV, IR or UV + IR absorption mode). The absorber harnesses all photons of energy greater than its bandgap.

The *solar irradiance spectrum* $\Phi_S(\lambda)$ is dependent on the irradiance condition S. In this study, S takes three label possibilities: S = 'AM 1.5G', 'monthly max.', and 'cloudy avg.', as defined in Fig. 3(c). For the sake of conciseness, S = AM 1.5G is abbreviated as S = 0. $\Phi_S(\lambda)$ can be divided into the UV (280–400 nm),

VIS (400–700 nm), and IR (700–4000 nm) regions. The spectral irradiance of AM 1.5G in the three regions can be written in the form

$$\varphi^r(\lambda) = \begin{cases} \Phi_0(\lambda), & \lambda_{\min}^r \le \lambda < \lambda_{\max}^r \\ 0, & \text{otherwise} \end{cases}, \qquad (1)$$

where $\lambda_{\min}^r$ and $\lambda_{\max}^r$ are the shortest and longest wavelengths in region r (r = UV, VIS, and IR). Note that $\Phi_0(\lambda)$ is the AM 1.5G spectrum. $\Phi_S(\lambda)$ can then be written as the weighted sum of irradiance in the three regions:

$$\begin{aligned} \Phi_S(\lambda) &= w_S^{UV}\varphi^{UV}(\lambda) + w_S^{VIS}\varphi^{VIS}(\lambda) + w_S^{IR}\varphi^{IR}(\lambda) \\ &= \sum_{r=UV,VIS,IR} w_S^r \varphi^r(\lambda), \end{aligned} \qquad (2)$$

where the weighting factor w_S^r is the relative intensity of spectrum S in region r compared to AM 1.5G (Fig. 3(b)). The values of w_S^r are given in Table S1 (ESI†).

The *harvestable irradiance spectrum* using a particular strategy G is denoted by $\tilde{\Phi}_{S;G}(\lambda)$. Here, G is a label for the STPV absorption strategy as depicted in Fig. 1(b). G can be one of the six strategies: {ND, UV}, {ND, IR}, {ND, UV, IR}, {BS, UV}, {BS, IR}, and {BS, UV, IR}. With these labels, analogous to eqn (2),

$$\begin{aligned} \tilde{\Phi}_{S;G}(\lambda) &= A_G^{UV}(\lambda)w_S^{UV}\varphi^{UV}(\lambda) + A_G^{VIS}(\lambda)w_S^{VIS}\varphi^{VIS}(\lambda) \\ &\quad + A_G^{IR}(\lambda)w_S^{IR}\varphi^{IR}(\lambda) \\ &= \sum_{r=UV,VIS,IR} A_G^r(\lambda)w_S^r\varphi^r(\lambda), \end{aligned} \qquad (3)$$

where $A_G^r(\lambda)$ is the absorptance (the fraction of incident irradiance absorbed) in the region r. Given six absorption strategies G and three spectral regions r, there are altogether 18 distinct $A_G^r(\lambda)$. Their detailed values or algebraic expressions are elaborated in the Section S1 (ESI†) and summarized in Table S2 (ESI†). Regarding visual perception, $A_G^{VIS}(\lambda)$ also determines the harvesting VIS α, the proportion of illuminance harnessed by the absorber, defined as

$$\text{Harvesting VIS} = \alpha\left(A_G^{VIS}(\lambda)\right) = \frac{\int_{400nm}^{700nm} A_G^{VIS}(\lambda)\varphi^{VIS}(\lambda)V(\lambda)d\lambda}{\int_{400nm}^{700nm} \varphi^{VIS}(\lambda)V(\lambda)d\lambda} \qquad (4)$$

where $V(\lambda)$ is the luminous efficiency function, which is the human eye sensitivity for different wavelengths of light.

The SQ-limited efficiency (eqn (S3), ESI†) for any irradiance condition S and strategy G can be evaluated from $\tilde{\Phi}_{S;G}(\lambda)$ derived in eqn (3) using procedures described in the previous work.[49] It predicts the theoretical max. PCE of an absorber with an optimal bandgap $E_{g,opt}$. An SQ-limited device assumes complete absorption above the absorber's bandgap (E_g) up to the designed transparency. Absorption is only undertaken in the absorber (active layer), *i.e.* fully transparent at all wavelengths for other device components. Every absorbed photon produces one excited electron–hole pair that undergoes thermal relaxation, possessing energy E_g (eqn (S4), ESI†). Some harnessed energy is dissipated from the detailed balance and fill factor

(eqn (S6) and (S9), ESI†).[49] The detailed formulation is given in Section S2 (ESI†).

The SQ-limited light utilization efficiency (LUE) is defined by

$$\text{LUE} = \text{PCE} \times \text{absorber AVT}. \qquad (5)$$

The absorber AVT ($\Upsilon_{S,G}$) in eqn (5) varies with the irradiance condition S and strategy G. It can be understood as the effective visible transmittance with a trimmed VIS range[50]

$$\begin{aligned} \text{Absorber AVT} &= \Upsilon_{S;G} \\ &= \frac{\int_{400nm}^{\min\left(700nm, \max\left(400, hc/E_{g,opt}\right)\right)}\left[1 - A_G^{VIS}(\lambda)\right]w_S^{VIS}\varphi^{VIS}(\lambda)V(\lambda)d\lambda}{\int_{400nm}^{700nm} w_S^{VIS}\varphi^{VIS}(\lambda)V(\lambda)d\lambda}, \end{aligned} \qquad (6)$$

where $E_{g,opt}$ is the optimal bandgap for the max. PCE; h and c are the Planck constant and the speed of light, respectively.

3. Results and discussion

3.1. Statistically derived maximum harvestable irradiance

3.1.1 Solar irradiance for semi-transparent photovoltaics in cities. In Fig. 4, the 16 cities are arranged based on their latitudes, and the average monthly maximum irradiance for each city over a period of 10 years (2013–2022) is divided into three wavelength ranges: UV (< 400 nm), VIS (400–700 nm), and IR (> 700 nm). The segmented data are then visualized as coloured bars, and the contribution of each wavelength range is depicted in the pie chart on the right. It is evident that IR constitutes approximately 50% to the total solar irradiance in most cities, followed by VIS at around 45%. The maximum IR irradiance values vary from 260–470 W/m² depending on the city's latitude and climate. On the other hand, UV has a maximum irradiance between 30–60 W/m², which is an order of magnitude lower than that of IR and VIS. It is shown that semi-/fully transparent photovoltaics utilizing an IR strategy offer the advantage of high maximum incident power.

6 cities were selected as examples as shown in Fig. 5, illustrating the irradiance values of different wavelength regions under varying cloud cover conditions in the box plot (left). The ESI† contains the same analysis for the remaining 10 cities. Under sunny sky conditions, the mean IR irradiance ranges between 250–350 W/m², whereas the mean UV irradiance remains around 35 W/m². This substantial difference in irradiance between IR and UV persists across all levels of cloudiness. In all studied cities, the mean IR irradiance remains above 100 W/m² during both sunny and mostly sunny conditions, which account for over 60% of occurrence in most cities over the course of ten years, as depicted in the pie chart adjacent to the box plot. On cloudy days, which occur approximately 10% of the time, the mean IR irradiance significantly drops to 40 W/m², and the mean UV irradiance decreases to below 10 W/m². However, even under these conditions, the amount of available solar power is still 10 times higher than that under 1000 lx indoor light (1 W/m²),[49] highlighting the potential for meaningful power generation through completely

This journal is © The Royal Society of Chemistry 2025

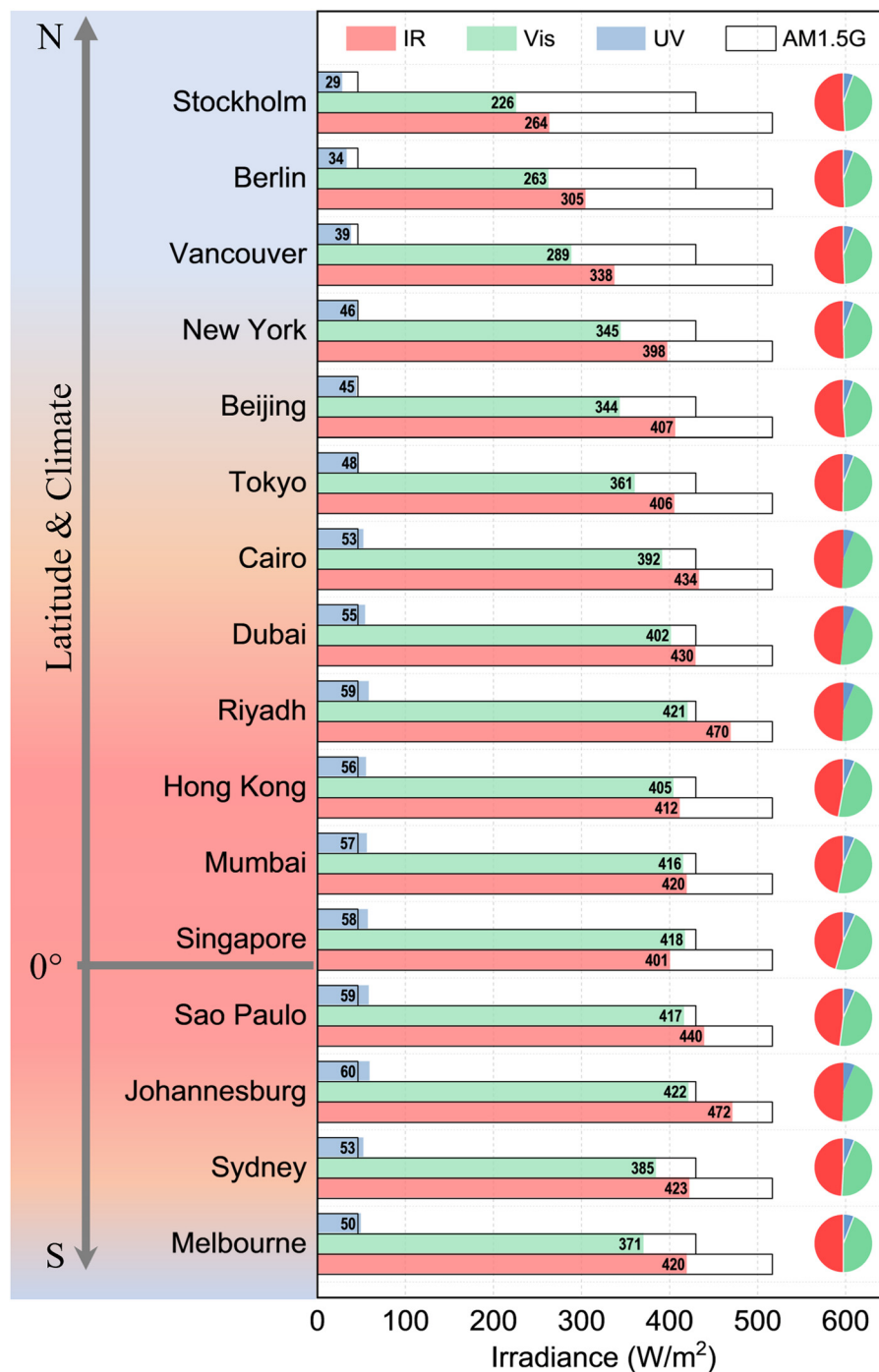*Energy Environ. Sci.*, 2025, **18**, 579–601 | **585**

Fig. 4 The monthly maximum solar irradiance data for each city, averaged over 10 years (2013–2022). The averages are segmented into three wavelength ranges: UV (<400 nm), VIS (400–700 nm), and IR (>700 nm), denoted by blue, green, and red bars, respectively. The black frame overlapping with each coloured bar represents the solar irradiance for that specific wavelength range in the AM 1.5G reference spectrum. The pie chart on the right illustrates the contribution of each wavelength region to the average monthly maximum irradiance.

transparent photovoltaics that absorb only IR or UV, even under overcast skies.

The stacked bars on the right side of Fig. 5 display the total mean irradiance under different cloud cover conditions and the percentage contribution of each wavelength range. It is evident that IR exhibits the highest contribution in most cities under sunny skies. However, its contribution decreases, and VIS becomes the dominant contributor in most cities under cloudy conditions. The contribution from UV remains relatively low, ranging between 5–8% under all conditions. This emphasizes the importance of absorbing a certain percentage of VIS if energy generation under cloudy skies is desired.
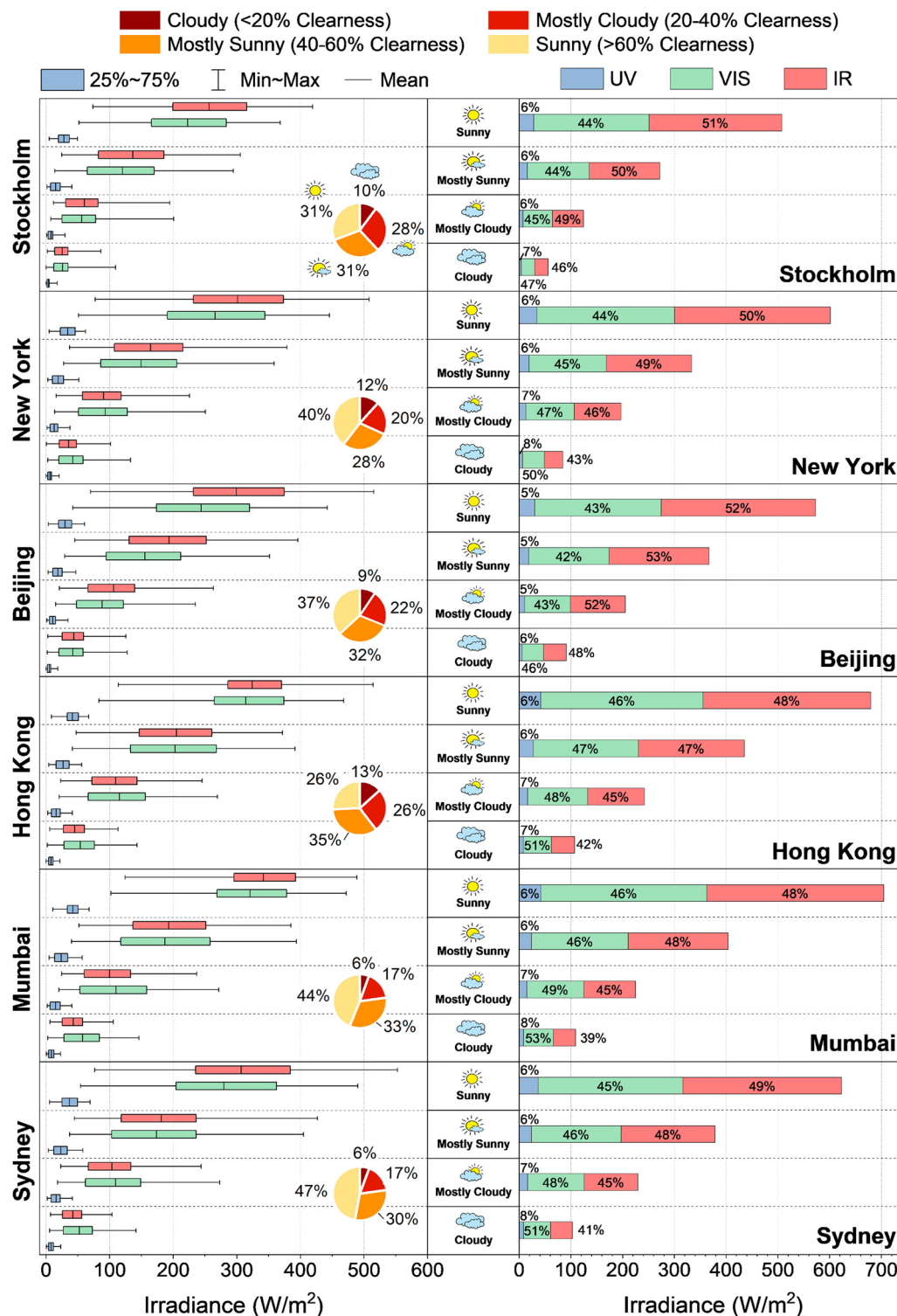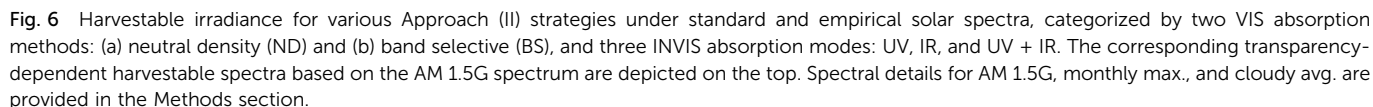
586 | *Energy Environ. Sci.,* 2025, **18**, 579–601

This journal is © The Royal Society of Chemistry 2025

Fig. 5 Solar irradiance analysis of 6 selected cities under different cloud cover conditions. The results are based on a 10-year dataset (2013–2022). The left box plot showcases the irradiance data at various wavelength ranges across varying cloudiness levels. The accompanying pie chart displays the distribution of cloud cover conditions during the analysed period. On the right, stacked bars represent the average total irradiance values under different cloud cover conditions, while the percentage contribution of each wavelength region is visualized. Fig. S2 and S3 (ESI†) include similar analyses for additional sets of 10 cities.

3.1.2 Harvestable irradiance for different absorption modulation strategies. Fig. 6 shows plots of harvestable irradiance under different cloud conditions and absorption modulation strategies. The plots were generated using the percentage of

This journal is © The Royal Society of Chemistry 2025

Energy Environ. Sci., 2025, **18**, 579–601 | **587**

Fig. 6 Harvestable irradiance for various Approach (II) strategies under standard and empirical solar spectra, categorized by two VIS absorption methods: (a) neutral density (ND) and (b) band selective (BS), and three INVIS absorption modes: UV, IR, and UV + IR. The corresponding transparency-dependent harvestable spectra based on the AM 1.5G spectrum are depicted on the top. Spectral details for AM 1.5G, monthly max., and cloudy avg. are provided in the Methods section.

'harvesting VIS' (x-axis) as the characteristic illuminance available for the absorber. The transparency levels can be defined by

0%—fully transparent; 100%—opaque; 30%—highly transparent; and 65%—translucent. In the ND strategy, harvesting VIS (%) can

be progressively reduced from 100% (opaque) to 0% (transparent) by lowering the harvestable spectral illuminance ($\tilde{\Phi}_{S;G}(\lambda)V(\lambda)$) in the VIS range as indicated in the upper 3 plots in Fig. 6(a). Similarly, in the BS strategy, harvesting VIS (%) can be gradually decreased from 100% to 0% by allowing selected spectral regions to become transparent as indicated in the upper 3 plots in Fig. 6(b). As examples, in a translucent {ND, IR} STPV, all IR is intended to be absorbed, while each colour light in the VIS range is to be absorbed by 65%. A translucent {BS, IR} STPV absorbs the full IR range together with VIS from 540–700 nm for power generation. By integrating the harvestable spectrum at various transparency levels for each strategy, their harvestable irradiance as a function of harvesting VIS (eqn (4)) under three spectra (AM 1.5G, monthly max., and cloudy avg.) are summarized below the harvestable spectra in Fig. 6. For the AM 1.5G spectrum, an opaque cell absorbing all light can harvest a maximum of 1000 W/m². As the percentage of harvesting VIS decreases, the irradiance intended for power generation is reduced. In the case of a fully transparent photovoltaic that absorbs UV and IR, the available irradiance diminishes to 570 W/m². These values decrease by nearly 20% for the monthly max. spectrum (458–826 W/m²) and over 90% for the cloudy avg. spectrum (48–95 W/m²). There are two methods for absorbing a specific percentage of VIS for a STPV: ND absorption, applied in Fig. 6(a); and BS absorption, employed in Fig. 6(b).

In Fig. 6(a), a linear drop in harvestable irradiance is observed as the harvesting VIS decreases across all three INVIS absorption modes and all three spectra. Under a sunny sky in cities (monthly max. spectrum, brown lines), the {ND, UV, IR} and {ND, IR} strategies yield a comparable harvestable irradiance of 776–826 W/m² for an opaque cell and 408–458 W/m² for a fully transparent cell. On the other hand, solar irradiance available for the {ND, UV} strategy is approximately half (418–476 W/m²) for an opaque cell and nearly one-tenth (46–50 W/m²) for a completely clear cell. The differences among three INVIS absorption modes are less obvious under a cloudy sky, with harvestable irradiance in the order of 10–100 W/m². Regarding STPV, a translucent {ND, IR} STPV that harnesses all IR and 65% ND VIS for power generation can leverage 647 W/m², while a highly transparent {ND, IR} cell that absorbs all IR and only 30% ND VIS has a harvestable irradiance of 518 W/m² under realistic sunny conditions.

In Fig. 6(b), percentage of VIS intended for power generation is selected based on wavelengths (BS VIS). The cutoff wavelength depends on the intended transparency of the cell. A translucent {BS, UV} STPV absorbs VIS from 400–575 nm in addition to all UV, whereas a highly transparent {BS, UV} STPV narrows the VIS absorption band to 400–540 nm, along with 100% UV absorption. Unlike the linear behaviour observed in the ND VIS absorption method, the BS VIS absorption method results in a non-linear fall as harvesting VIS reduces. The non-linearity mainly originates from the bell shape of the luminous efficiency function $V(\lambda)$, where the two ends of the VIS spectrum have a lower spectral sensitivity to human visual perception.

Among the three INVIS absorption modes, {BS, UV, IR} showcases the highest harvestable irradiance, closely followed

by {BS, IR}, while both significantly outperform {BS, UV}. In comparison to {ND, IR} in Fig. 6(a), a translucent {BS, IR} cell has 45 W/m² lower harvestable irradiance (602 W/m²) under urban sunny conditions. However, a highly transparent {BS, IR} PV can enjoy a higher solar irradiance than that of {ND, IR}, with an increase of 34 W/m² (to 552 W/m²). This indicates that the BS method is more favourable for high-transparency STPV applications.

These results form the foundation for estimating the performance limits of various absorption modulation strategies for STPVs in subsequent analyses.

3.2. Maximum power output

The maximum possible PCE of any solar cell is always a benchmark of universal interest.[49,51,52] Here, we expand upon Lunt's work on 'UV/NIR wavelength-selective' limiting PCE[26] (which we designate as {ND, UV, IR} in this work) by (1) incorporating realistic irradiance conditions (*i.e.* monthly max. and cloudy avg.), (2) allowing for different INVIS absorption modes (UV, IR and UV + IR), and (3) including the BS method (which is widely adopted by both organic and broadband inorganic STPVs). The BS method modulates the colour of the transmitted light, offering potential aesthetic features. We suggest material parameters for optimal energy-brightness performance for different absorber AVTs and compare the performance using the six strategies as a combination of the three INVIS absorption modes and two VIS absorption methods. The calculated maximum PCE, output power intensity, and LUE serve as a reference of estimate for various cities.

3.2.1 Limiting efficiency and output power intensity. Fig. 7 shows the SQ-limited PCE (see Section 2.2) and the corresponding output power intensities at different absorber AVT values (eqn (6)) in various scenarios. Each row in Fig. 7 corresponds to an irradiance condition with its solar irradiance P_{in}. The top row (Fig. 7(a) and (b)) shows the results under the AM 1.5G spectrum (P_{in} = 1000 W/m²). The middle (Fig. 7(c) and (d)) and the bottom (Fig. 7(e) and (f)) rows depict the results under the monthly max. and the cloudy avg. irradiance conditions, which are derived from AM 1.5G with different irradiance proportions in the UV, VIS, and IR regions (see Fig. 3(b), eqn (2) and Table S1 for the composition and proportions, ESI†). These two empirical spectra represent the realistic maximum irradiance in cities under a sunny sky (P_{in} = 826 W/m²) and the average irradiance under an overcast sky (95 W/m²).

The maximum possible PCE generally decreases with higher absorber transparency, primarily due to the declining harvestable irradiance (Fig. 6), and thus, the output power intensity. Note the same values at 0% and 100% absorber AVT for an absorption mode under a specific irradiance condition. In Fig. 7(a), our {ND, UV, IR} strategy under AM 1.5G recovers the 'wavelength-selective' strategy previously reported,[25,26] where the max. PCE drops from 33% at 0% absorber AVT (opaque, the conventional solar cells)[51] to 19% at 100% absorber AVT (fully transparent). The subtle difference originates from the wavelength range for the VIS region (400–700 nm defined here *vs.* 435–670 nm). The maximum possible PCEs at
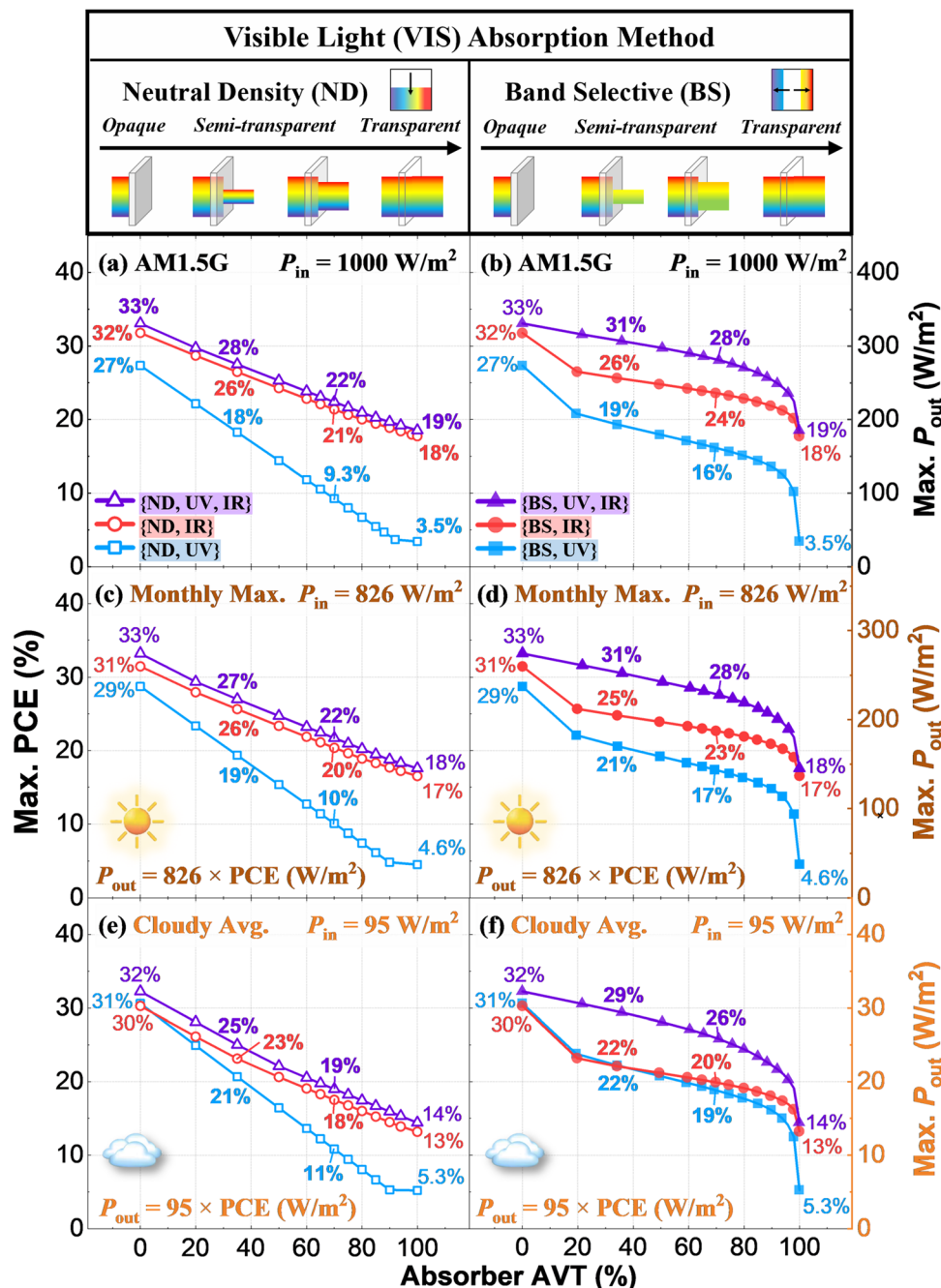
This journal is © The Royal Society of Chemistry 2025

Energy Environ. Sci., 2025, **18**, 579–601 | **589**

Fig. 7 The Shockley–Queisser-limit PCE (left axes) and the corresponding max. P_{out} (right axes) vs. absorber AVT under the AM 1.5G (top row, a and b), monthly max. (centre row, c and d), and cloudy avg. (bottom row, e and f) irradiance conditions using the neutral density (ND, left panel, a, c and e) and the band selective (BS, right panel, b, d and f) methods. The harvestable power intensity (P_{in}) and the corresponding max. P_{out} are stated in each row of irradiance conditions. In each subfigure, the colors and symbols represent the three INVIS absorption modes (UV + IR: purple triangles; IR: red circles; UV: blue squares), with the max. PCE values annotated for specific AVT levels (0% opaque, 35% translucent, 70% highly transparent, 100% fully transparent). The corresponding max. P_{out} values are tabulated in Table 1. Within each row, the harvestable irradiance spectra of the ND and BS methods at 0% and 100% absorber AVT are identical, respectively. The {ND, UV, IR} curve in (a) mimics the 'wavelength-selective' strategy[26] up to the range of wavelength. Note the same max. PCE scales (left axes) but distinct max. P_{out} scales (right axes) across the rows.

four representative absorber AVTs are annotated: opaque (0%), translucent (35%), highly transparent (70%), and fully transparent (100%). These values and the maximum output power intensities are tabulated in Table 1. A translucent STPV device (35% absorber AVT) can achieve a max. PCE of 18–22%, 22–26%

and 25–31% for the UV (blue), IR (red) and UV + IR (purple) absorption modes, respectively. As a remark, the max. PCE under the AM 1.5G and empirical monthly max. irradiance conditions are numerically proximate for the UV + IR (purple, <1%) and IR absorption modes (red, <1.2%) irrespective of

Table 1 The maximum power conversion efficiency (PCE), output power intensity (P_{out}), light utilization efficiency (LUE), and the range of bandgaps that enable over 90% max. PCE for different VIS absorption methods M across the columns: neutral density (ND) and band selective (BS), and INVIS absorption modes (across the rows): UV, IR and UV + IR, under various irradiance conditions (AM 1.5G, monthly max. and cloudy avg.) at 0% (opaque), 35% (translucent), 70% (highly transparent), and 100% (fully transparent) absorber average visible transmittance (AVT). The range of bandgaps is given by the lowest value reaching max. PCE = 90% ($E_{g,lower}$), the optimal value achieving the highest PCE ($E_{g,opt}$), and the highest value reaching max. PCE = 90% ($E_{g,upper}$)

Absorber AVT (%)	Irradiance condition	Neutral density (M = ND)				Band selective (M = BS)			
		PCE (%)	P_{out} (W/m²)	LUE (%)	$E_{g,lower}$–$E_{g,opt}$–$E_{g,upper}$ for PCE > 90% (eV)	PCE (%)	P_{out} (W/m²)	LUE (%)	$E_{g,lower}$–$E_{g,opt}$–$E_{g,upper}$ for PCE > 90% (eV)
UV Mode {M, UV}									
0	AM 1.5G	27	270	0	1.63–1.77–1.91	27	270	0	1.63–1.77–1.91
	Monthly max.	29	240	0	1.63–1.77–1.91	29	240	0	1.63–1.77–1.91
	Cloudy avg.	31	29	0	1.63–1.77–1.92	31	29	0	1.63–1.77–1.92
35	AM 1.5G	18	180	6.4	1.63–1.77–1.92	19	190	6.7	1.97–2.15–2.25
	Monthly max.	19	160	6.8	1.63–1.77–1.93	21	170	7.1	1.97–2.15–2.25
	Cloudy avg.	21	20	7.2	1.63–1.77–1.93	22	21	7.6	1.98–2.15–2.26
70	AM 1.5G	9.3	93	6.5	1.63–1.77–1.95	16	160	11	2.11–2.30–2.39
	Monthly max.	10	83	7.1	1.63–1.77–1.98	17	140	12	2.11–2.30–2.40
	Cloudy avg.	11	10	7.6	1.64–1.77–1.99	19	18	13	2.12–2.30–2.40
100	AM 1.5G	3.5	35	3.5	2.84–3.10–3.16	3.5	35	3.5	2.82–3.09–3.14
	Monthly max.	4.6	38	4.6	2.83–3.10–3.16	4.6	38	4.6	2.82–3.09–3.15
	Cloudy avg.	5.3	5	5.3	2.84–3.10–3.16	5.3	5	5.3	2.83–3.09–3.15
IR Mode {M, IR}									
0	AM 1.5G	32	320	0	0.92–1.34–1.59	32	320	0	0.92–1.34–1.59
	Monthly max.	31	260	0	0.94–1.34–1.65	31	260	0	0.94–1.34–1.65
	Cloudy avg.	30	29	0	1.08–1.39–1.80	30	29	0	1.08–1.39–1.80
35	AM 1.5G	26	260	9.3	0.90–1.13–1.44	26	260	8.8	0.89–1.13–1.42
	Monthly max.	26	210	9.0	0.90–1.13–1.47	25	200	8.5	0.90–1.13–1.45
	Cloudy avg.	23	22	8.1	0.94–1.34–1.58	22	21	7.6	0.93–1.14–1.55
70	AM 1.5G	21	210	15	0.87–1.12–1.26	24	240	16	0.88–1.12–1.38
	Monthly max.	20	170	14	0.88–1.12–1.27	23	190	16	0.89–1.12–1.40
	Cloudy avg.	18	17	12	0.90–1.12–1.39	20	19	14	0.91–1.13–1.46
100	AM 1.5G	18	180	18	0.86–0.94–1.18	18	180	18	0.86–0.94–1.19
	Monthly max.	17	140	17	0.87–0.94–1.19	17	140	17	0.87–0.94–1.19
	Cloudy avg.	13	13	13	0.87–0.95–1.21	13	13	13	0.87–0.95–1.21
UV + IR Mode {M, UV, IR}									
0	AM 1.5G	33	330	0	0.93–1.34–1.62	33	330	0	0.93–1.34–1.62
	Monthly max.	33	270	0	0.97–1.38–1.69	33	270	0	0.97–1.38–1.69
	Cloudy avg.	32	31	0	1.09–1.39–1.85	32	31	0	1.09–1.39–1.85
35	AM 1.5G	28	280	9.6	0.90–1.13–1.47	31	310	11	0.91–1.14–1.57
	Monthly max.	27	220	9.5	0.91–1.13–1.51	31	250	11	0.93–1.34–1.61
	Cloudy avg.	25	24	8.8	0.98–1.34–1.64	29	28	11	1.08–1.39–1.78
70	AM 1.5G	22	220	16	0.88–1.12–1.28	28	280	20	0.90–1.13–1.48
	Monthly max.	22	180	15	0.88–1.12–1.37	28	230	20	0.91–1.14–1.53
	Cloudy avg.	19	18	13	0.91–1.13–1.43	26	25	18	1.01–1.38–1.66
100	AM 1.5G	19	190	19	0.86–0.95–1.20	19	190	19	0.86–0.95–1.20
	Monthly max.	18	150	18	0.87–0.95–1.21	18	150	18	0.87–0.95–1.21
	Cloudy avg.	14	14	14	0.88–1.12–1.24	14	14	14	0.88–1.12–1.24

This journal is © The Royal Society of Chemistry 2025

Energy Environ. Sci., 2025, **18**, 579–601 | **591**

the ND or BS method (Fig. 7(a), (c) and (b), (d)). Therefore, the standard AM 1.5G irradiance condition could be a convenient approximation to monthly max. (the sunniest weather) for PCE estimation.

Besides PCE, Fig. 7 (right axes) also depicts the maximum P_{out}, the product of the maximum possible PCE given by the left axis and P_{in} indicated in that row of irradiance conditions. From Fig. 7(c) and (d), the values for monthly max. are ~80% of AM 1.5G with the UV + IR and IR absorption modes for both the ND and BS methods. An opaque device (0% absorber AVT) under realistic sunny conditions might generate 270 W/m^2 instead of 330 W/m^2 under AM 1.5G with the UV + IR absorption mode (Fig. 7(a) and (b)) despite the similar maximum possible PCE of 33%. Similarly, cloudy avg. with an even lower P_{in} (95 W/m^2) might allow for a maximum P_{out} of 31 W/m^2 with a maximum possible PCE of 32% (Fig. 7(e) and (f)). Nonetheless, the energy generated under the cloudy weather is still more than tenfold that from indoor photovoltaics (e.g. 1.6 W/m^2 under 1000 lx from an LED lamp[49]). As a rough estimate, a typical narrowband-internet of things (NB-IoT) device that consumes a 5 Wh battery in 270 days[53] could be powered by a 1.1 cm^2 highly transparent solar cell (70% absorber AVT) using the {ND, IR} strategy without a solar concentrator, assuming an equivalence irradiance of 10-hour cloudy avg. per day[42] (P_{out} = 17 W/m^2 from Fig. 7(e)). As such, a STPV may provide more than sufficient energy for driving small IoT devices.

For both the ND and BS methods, the UV + IR absorption mode (purple) enables the most efficient electricity production, closely followed by the IR (red) mode. The UV + IR absorption mode (purple) can convert up to ~150 W/m^2 (Fig. 7(a) and (b)), ~110 W/m^2 (Fig. 7(c) and (d)), and ~10 W/m^2 (Fig. 7(e) and (f)) more than the UV mode (blue) for the AM 1.5G, monthly max., and cloudy avg. irradiance conditions, respectively. Compared to the IR mode, the UV + IR mode (purple) also allows up to >30% more output power intensity.

The ND method (left) exhibits a linear decrease in max. PCE with increasing absorber AVT. Such a drop is faster in the UV mode than in IR and UV + IR modes: 2.6–2.8% vs. 1.4–1.8% per 10% absorber AVT (see also Table S3, ESI†). On the other hand, the BS method (right) experiences a relatively steady decline for all modes in the moderate-to-high absorber transparency range (20–85%). Such a feature enables a superior STPV performance using the BS strategy at the moderate-to-high absorber AVT (>50%). A highly transparent absorber (70% absorber AVT) with the UV mode benefits significantly from the BS method: the max. PCE drops to 9.3–11% and 16–19% for {ND, UV} (left, blue) and {BS, UV} (right, blue), differing by 7–8%. The IR (red) and UV + IR (purple) modes also exhibit appreciable differences: 18–21% and 20–24% for {ND, IR} (left, red) and {BS, IR} (right, red), and 19–22% and 26–28% for {ND, UV, IR} (left, purple) and {BS, UV, IR} (right, purple). Consequently, a highly transparent STPV device using the BS method produces higher P_{out}, achieving a maximum value of 140–160 (18) W/m^2 using {BS, UV} (right, blue) under the AM 1.5G and monthly max. (cloudy avg.) irradiance, significantly higher than {ND, UV}

(left, blue; 83–93 (10) W/m^2), as shown in Table 1. The difference is also noticeable when comparing {ND, IR} (left, red; 170–210 (17) W/m^2) and {BS, IR} (right, red; 190–240 (19) W/m^2), and comparing {ND, UV, IR} (left, purple; 180–220 (18) W/m^2) and {BS, UV, IR} (right, purple; 230–280 (25) W/m^2).

{BS, UV, IR} is the outstanding strategy among all because this strategy prioritizes the brightest photons for transparency, i.e. wavelength of large $V(\lambda)$, leaving the most photons for power generation while also harnessing UV and IR. It allows for a maximum P_{out} over 200 (20) W/m^2 with a max. PCE over 25% (22%) under the monthly max. (cloudy avg.) (purple, Fig. 7(d) and (f)) irradiance condition even for an absorber with 90% AVT. In contrast, devices using the UV absorption mode (blue lines) suffer from failure to harness high-irradiance IR photons (see Fig. 3(d)), leading to photon underutilization, a large decline rate of PCE and P_{out} with respect to the absorber AVT (Table S3, ESI†), and poor limiting performance at high absorber AVT. Therefore, IR absorption is essential for efficient STPVs; the UV absorption mode is undesirable for high-transparency STPV applications.
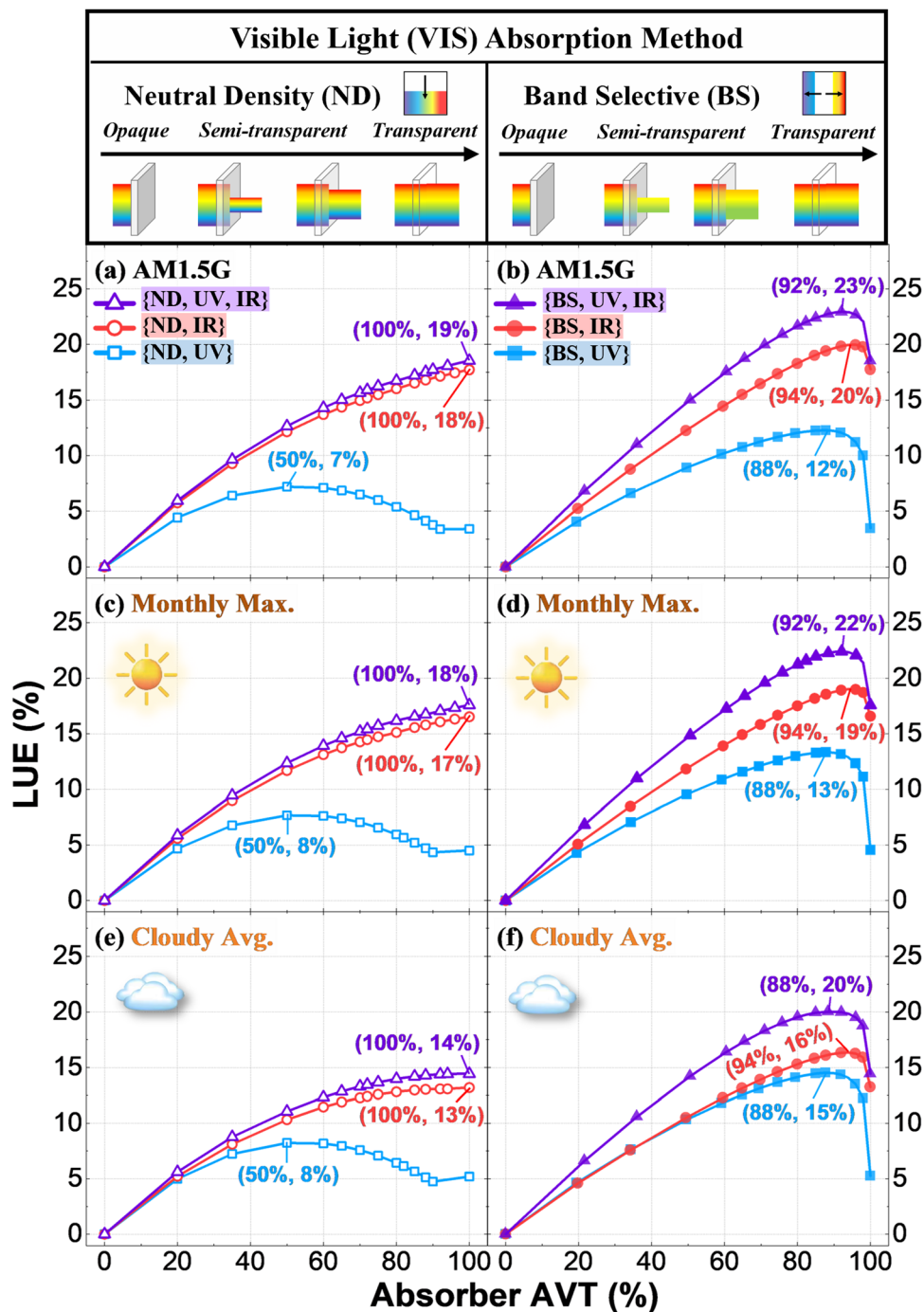
3.2.2 Limiting light utilization efficiency (LUE). LUE (eqn (5)) is a metric to assess an STPV device's effectiveness of simultaneous energy harvesting and visual perception performance, characterised by PCE and AVT, respectively. It encapsulates the competition between AVT and PCE since PCE generally decreases with AVT (see Fig. 7). A maximum possible PCE at a particular AVT implies a maximum LUE at that AVT. Fig. 8 shows the PCE-optimal LUE using different strategies under the three irradiance conditions (rows), with values of representative absorber AVT tabulated in Table 1. Since LUE is a function of PCE, which varies with the harvestable irradiance spectra, LUE depends on the extrinsic (irradiance spectra) and intrinsic (absorber absorption methods and modes) conditions. A high-LUE device absorbs light not sensitive to human eyes (wavelengths of low $V(\lambda)$) and transmits bright photons.

{ND, UV, IR} and {ND, IR} give a monotonic increasing LUE with the absorber AVT (purple and red curves in Fig. 8(a), (c) and (e)). Others show an intermediate optimal (annotated in Fig. 8). UV absorption mode achieves the maximum LUE at 50% absorber AVT for the ND method (left panel, blue) and at 88–94% for the BS method (right panel, blue). Therefore, {ND, UV} is optimised for moderately transparent applications. Still, its LUE is not as competitive as its BS counterpart. The other five strategies are particularly advantageous for high-transparency applications. Given the drastic LUE drop for the BS method after the optimal absorber AVT, absorbers adapting the BS method should limit their AVT to around 90%.

Absorbers of AVT > 50% generally achieve higher LUE using the BS method (right) than the ND (left) for all absorption modes under all irradiance conditions, thanks to BS's more efficient photon utilization at such transparencies that maintains a high PCE with a slow decline with the absorber AVT (Fig. 7). In particular, the property of the BS method that achieves high PCEs across a broad absorber AVT range allows a sharper LUE increase with absorber AVT and thus higher LUEs. The maximum possible LUE using {BS, UV, IR}, i.e. the

592 | Energy Environ. Sci., 2025, **18**, 579–601

This journal is © The Royal Society of Chemistry 2025

Fig. 8 The max. LUE *vs.* AVT under the AM 1.5G (top row, a and b), monthly max. (centre row, c and d), and cloudy avg. (bottom row, e and f) irradiance conditions using the neutral density (ND, left panel, a, c and e) and the band selective (BS, right panel, b, d and f) methods. In each subfigure, the results using the three absorption modes (UV only (blue squares), IR only (red circles), and UV + IR (purple triangles)) are displayed alongside their peak values in ordered pairs (*absorber AVT, max. LUE*). Table S4 (ESI†) summarizes the range of peak values for each strategy (VIS absorption methods and INVIS absorption modes). The LUE values at representative transparency are tabulated in Table 1.

purple curves, under AM 1.5G and monthly max. (cloudy avg.) can reach 22–23% (20%), while that using {ND, UV, IR} is 18–19% (14%) only. The BS method surpasses the ND counterpart by 4–6%. The difference also exists in the IR (red, 2–3%) and UV (blue, 5–7%) absorption modes. Regarding all irradiance conditions, {BS, UV, IR} allows for the best maximum LUE

because of its prior utilization of bright photons for visual perception and the rest for power generation (Table S4, ESI†). It is important to note that the theoretical max. LUE presented here is based on the absorber AVT. In practice, the AVT of other functional layers, such as electron transporting layers and electrodes, can significantly reduce the overall device AVT,
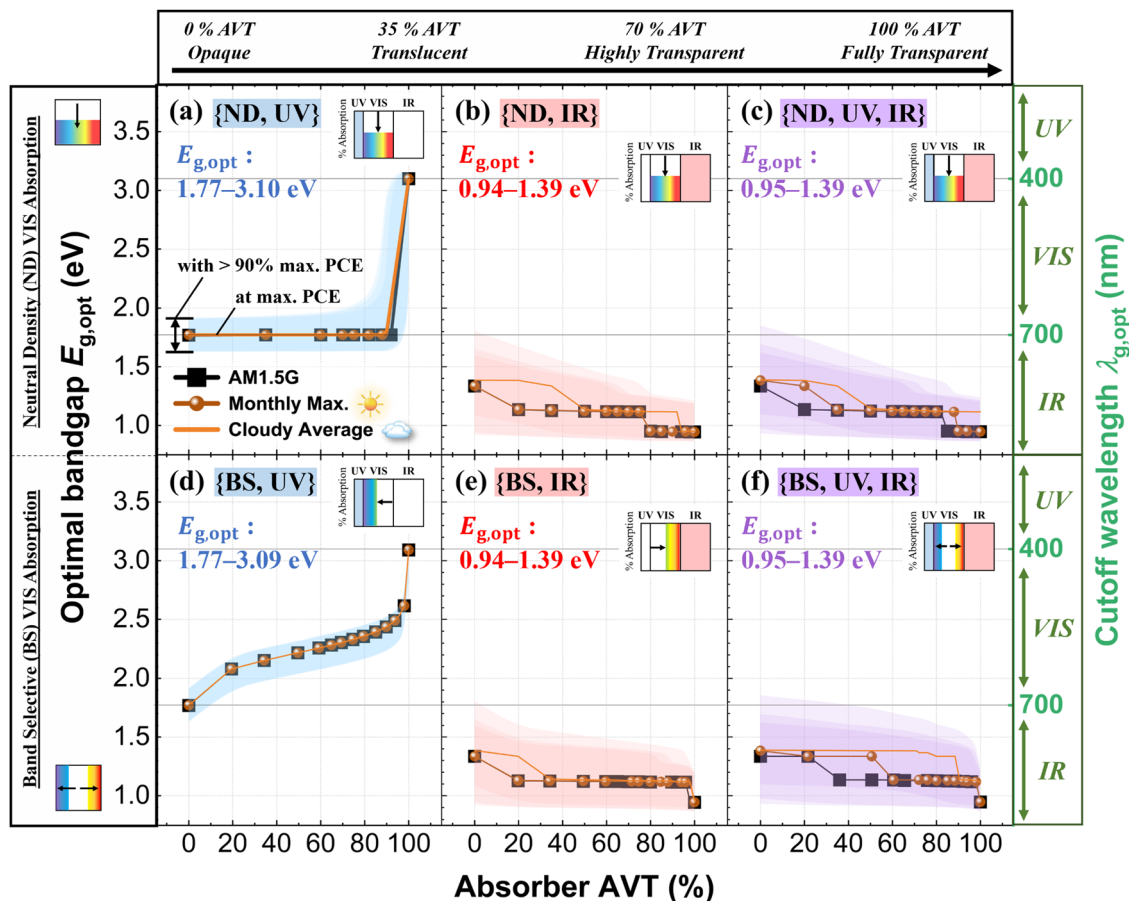
This journal is © The Royal Society of Chemistry 2025

Energy Environ. Sci., 2025, **18**, 579–601 | **593**

Fig. 9 The PCE-optimal bandgap ($E_{g,opt}$) *vs.* AVT over the three irradiance conditions (AM 1.5G, monthly max. and cloudy avg.) for the neutral density (ND, top row, a–c) and band selective (BS, bottom row, d–f) methods and the UV (left column, a and d), IR (middle column, b and e), and UV + IR (right column, c and f) absorption modes. The lines refer to the bandgap for the max. PCE. The shaded regions correspond to the range of bandgaps where the limiting PCE reaches over 90% of the maximum value. Regions of deeper colours as the overlap of those corresponding to various irradiance conditions indicates higher confidence levels. A wider bandwidth characterizes a higher tolerance of bandgaps for optimal STPV performance.

limiting the device's LUE. Further discussion on the impact of these functional layers on device performance and transparency is provided in Section 3.3.

3.2.3 Material parameter—optimal bandgap. The STPV performance for a given absorber AVT needs to strive for an optimal balance between the subgap loss and thermal relaxation by modulating the bandgap E_g. Fig. 9 depicts the PCE-optimal bandgap variation with absorber AVT using different strategies of absorption modes and methods. The solid lines denote the bandgap at the SQ-limited PCE ($E_{g,opt}$). The shaded area represents the range of E_g that allows for PCE over 90% of the SQ-limited value (*e.g.* a maximum PCE of 20% spans the range of 18–20%) under each irradiance condition. Deeper shades result from the overlap of the shades corresponding to different irradiance conditions, indicating a greater confidence level of spectral variation, *i.e.* the bandgap range has a broader spectral applicability. A large vertical range signifies a large bandgap tolerance that allows absorber materials of diverse E_g to achieve high PCE. The bandgap ranges at representative absorber AVTs are tabulated in Table 1.

For most strategies, $E_{g,opt}$ is similar under the three irradiance conditions. The IR and UV + IR absorption modes have a

stable $E_{g,opt}$ regardless of transparency and the absorption method (ND or BS), with a typical value of 0.9–1.4 eV (890–1380 nm) at absorber AVT > 20% to maintain > 90% max. PCE (Fig. 9(b), (c), (e) and (f)). The tolerance is generally smaller at high transparency (≈ 0.3 eV). Nonetheless, some inorganic materials absorb UV and cannot accommodate the IR mode without strong VIS absorption. The range of the optimal bandgap using {UV, ND} (Fig. 9(a)) is generally located around the red-end VIS (1.77 eV or 700 nm) and permits the entire VIS range at 90–94% absorber AVT. The lower bound is shifted to 2.8 eV (440 nm) at 100% absorber AVT. For {BS, UV} (Fig. 9(d)), the typical value lies at 2.1–2.4 eV (520–590 nm) at 20–90% absorber AVT.

3.2.4 Summary of absorption modulation strategy comparison. Fig. 10 summarizes the SQ-limited LUE and PCE variations for different strategies over the three irradiance conditions in this study. The shaded regions denote the possible maximal performance achieved, derived from max. PCE and LUE presented in Fig. 7 and 8, respectively. The slope at any point ($y:x$ ratio) represents the absorber AVT (see eqn (5)). Strategies covering the top-right corner can archive high PCE
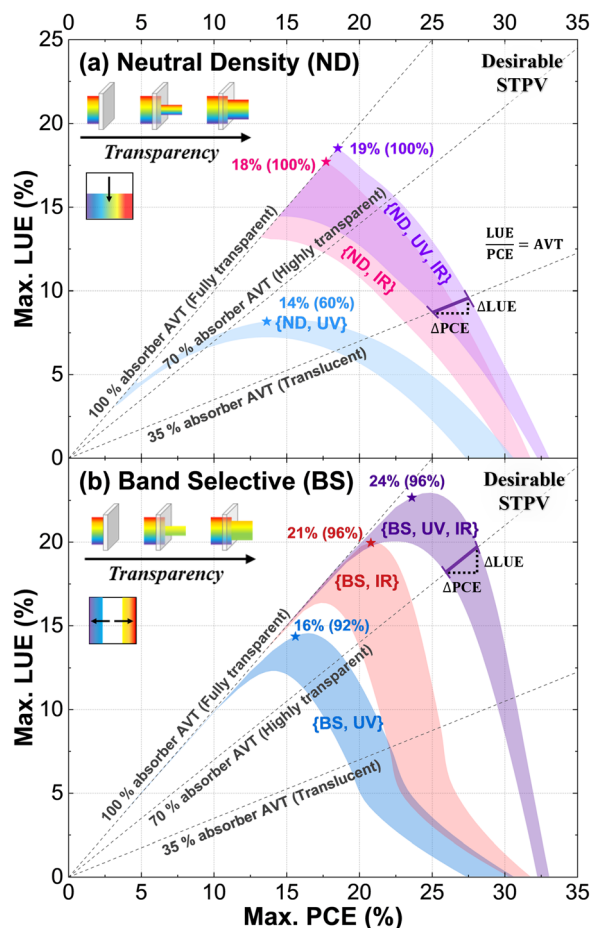
Fig. 10 Summary plot of maximum LUE *vs.* max. PCE for the (a) neutral density (ND) and (b) band selective (BS) methods. The shaded region depicts the possible performance achieved by that strategy (over the three irradiance conditions in this study: AM 1.5G, monthly max. and cloudy avg.). Strategies capable of achieving simultaneous high-PCE and high-LUE are preferred (top right). Three typical transparencies (100%—fully transparent, 70%—highly transparent, and 35%—translucent) are shown in dashed lines. The upper end of the dashed lines in a shaded region indicates the best performance achievable by that strategy. The width along an AVT contour denotes the performance variance at that AVT; its horizontal and vertical projections are the PCE and LUE ranges for that absorber AVT. The stars represent the optimal operating conditions for the strategy, indicated by the label max. PCE (absorber AVT). Note that the region above the 100% absorber AVT contour corresponds to absorber AVT > 100%, thus not occupied by any strategy.

and LUE *simultaneously*, and thus are potential high-performance STPV candidates. Among the six strategies, {BS, UV, IR} (purple, Fig. 10(b)) is outstanding. It enables a maximum possible PCE of 14–33% (range on the *x*-axis). Under the realistic sunny sky, a maximum output power intensity (P_{out}) of 150–250 W/m^2 can be delivered, and the highest LUE of 23% (maximum *y* value) can be achieved at 92% absorber AVT (*y* : *x* ratio).

For moderately to highly transparent STPV applications, the BS method (Fig. 10(b)) is generally preferred given a particular absorption mode because of its higher achievable PCE, P_{out}, and LUE (more top right). Devices with IR absorption (IR (red)

and UV + IR (purple) modes) are comparatively efficient, with an optimal bandgap of 0.94–1.39 eV. If the UV absorption mode has to be employed, materials with an optimal bandgap of 2.2–2.5 eV using {BS, UV} (blue, Fig. 10(b)) is more preferrable than {ND, UV} (blue, Fig. 10(a)).

The width along an AVT contour in the shaded region indicates the performance variance at that AVT. A smaller bandwidth implies smaller PCE and LUE ranges and more stable performance with irradiance condition variations. For example, at 70% absorber AVT, {BS, UV, IR} (purple, Fig. 10(b)) maintains a more stable PCE and LUE with respect to various irradiance conditions, achieving 26–28% PCE and 18–20% LUE, compared to 20–24% PCE and 14–17% LUE for {BS, IR} (red, Fig. 10(b)). In general, regarding high-performance STPV, {BS, UV, IR} (purple, Fig. 10(b)) is more tolerating for different irradiance conditions compared to other IR (red) and UV + IR (purple) absorption modes, especially at high AVT. The stars in Fig. 10 denote the optimal operating conditions for the strategy. The optimal conditions are conventionally defined by the maximal AVT (slope) and the Euclidean distance from the origin. {ND, UV} is optimal at moderate absorber AVT (60%); others work well at very high transparency. {BS, UV, IR} performs optimally at 96% absorber AVT, with a max. PCE of 24%.

3.3. Effects of other functional layers

Functional layers, apart from the active layer, such as charge transporting layers, electrodes, and encapsulants, have a significant impact on the device's PCE and AVT.[38,39,54,55] The transmittance of common functional layers for STPVs is shown in Fig. 11. The data are extracted from various literature sources, and the corresponding AVT values are calculated and listed in Table 2 along with their sources. This table can be used to roughly estimate the cumulative impact of other functional layers on the overall AVT of the device. By considering the example of glass/ITO/PEDOT:PSS/absorber/ZnO/Ag nanowires, we can calculate the approximate device AVT as the product of the individual layer transmittances.[56] The device AVT is given by 0.874 × 0.885 × 0.915 × 0.941 × absorber's AVT = 0.666 × absorber's AVT. Therefore, the highest achievable AVT for this device is 66.6% when the absorber layer is 100% transparent, assuming that there are no inter-layer interference and no specialized optical engineering to enhance transmission. This demonstrates that the overall device LUE is governed not only by the absorber AVT but also by the AVT of other functional layers.

In Fig. 11(a), the transmittance of non-metal charge extraction layers, including carrier transporting layers and electrodes, is summarized. These layers exhibit a high AVT of 80–90%. However, some of them, such as spiro-OMeTAD and ZnO, are less transparent or even opaque to UV. Using these layers as intermediates for UV mode STPVs can significantly attenuate the UV reaching the active layer, thus affecting the device's PCE and bi-facial functionality. Limited information is available regarding the transmittance of these layers to IR. Considering that nearly 99% of IR irradiance falls within the near-IR (NIR) range, it is advisable to evaluate the transmittance of these
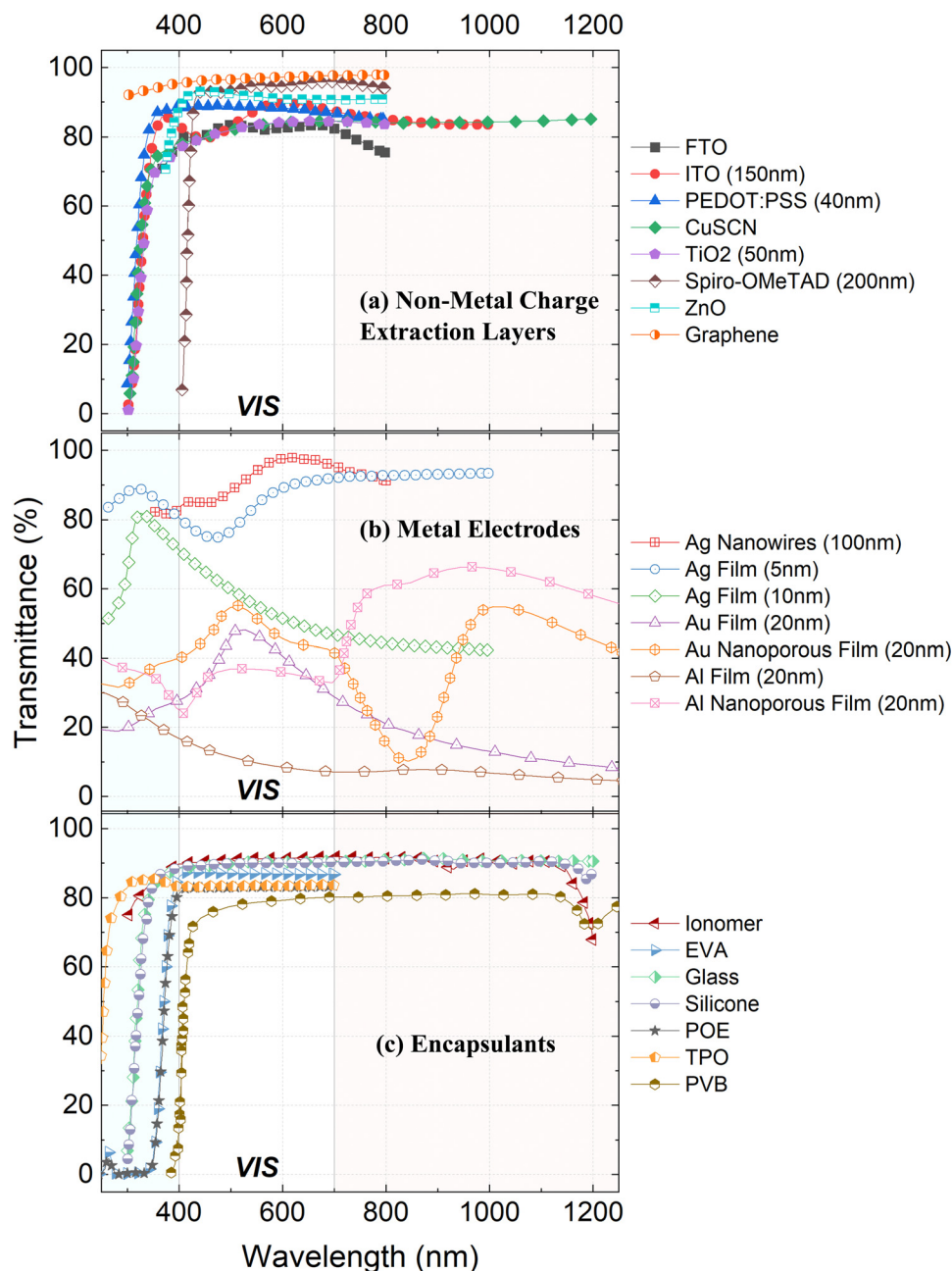
This journal is © The Royal Society of Chemistry 2025

Energy Environ. Sci., 2025, **18**, 579–601 | **595**

Fig. 11 Transmission spectra of common functional layers for semi-transparent photovoltaics extracted from various sources as specified in Table 2: (a) non-metal charge extraction layers; (b) metal electrodes; and (c) encapsulants.

layers in the 700–2500 nm (NIR) region before incorporating them into STPVs.

Fig. 11(b) reveals that the AVT of metal electrodes can vary significantly depending on their thickness and nanostructures. Generally, uniform metal films with thicknesses exceeding 10 nm exhibit AVT below 60%, making them critical layers that govern the device's AVT. Metal films with low AVT may also show similar transmittance in the INVIS, adversely affecting the device's PCE. For instance, a 20 nm aluminium film has an AVT as low as 10% and is nearly opaque to IR. However, AVT can be improved by reducing the thickness (to <10 nm) or

introducing nanostructures like nanowires or nanoholes. By reducing the thickness of a silver film from 10 nm to 5 nm, its AVT can increase from 54.7% to 84.5%. The introduction of nanoholes to 20 nm gold and aluminium films enhances their AVT. Among the various methods for improving the AVT of metal electrodes, silver nanowires give the highest AVT of 94.1%, even with a thickness of 100 nm.

All reported encapsulants have high AVT (80–90%), indicating minimal concerns regarding the transparency of STPVs (Fig. 11(c)). However, some encapsulants may have limited transmittance in the INVIS, which can severely affect the

Table 2 AVT of common functional layers for semi-transparent photovoltaics: non-metal charge extraction layers, metal electrodes, and encapsulants. AVT values are calculated based on the transmission spectra from various sources, as specified in the table. The transmission spectra of these functional layers can be found in Fig. 11

Material	Thickness	Substrate	Total AVT^a (%)	Source
Non-metal charge extraction layers				
FTO	—	Glass	82.7 (82.7)	57
ITO	150 nm	Glass	87.4 (87.4)	58
PEDOT:PSS	40 nm	—	88.5 (88.5)	59
CuSCN	—	Glass	83.3 (83.3)	60
TiO$_2$	50 nm	—	83.4 (83.4)	61
Spiro-OMeTAD	200 nm	Glass	94.4 (94.4)	62
ZnO	—	Glass/ITO	91.5 (91.5)	63
Graphene	—	Glass	97.0 (97.0)	63
Metal electrodes				
Ag nanowires	100 nm	Glass/ITO	94.1 (94.1)	64
Ag film	5 nm	Quartz	84.5 (84.5)	65
Ag film	10 nm	Quartz	54.7 (54.7)	65
Au film	20 nm	—	44.0 (44.0)	66
Au nanoporous film	20 nm	—	50.0 (50.0)	66
Al film	20 nm	—	9.6 (9.6)	66
Al nanoporous film	20 nm	—	36.4 (36.4)	66
Encapsulants				
Ionomer	1.97 mm	—	91.3 (91.3)	67
EVA	0.43 mm	—	87.0 (87.0)	67
Glass	3.2 mm	—	90.3 (90.3)	68
Silicone	<1 mm	Glass	90.0 (90.0)	68
POE	0.45 mm	—	83.0 (83.0)	69
TPO	0.45 mm	—	83.4 (83.4)	69
PVB	0.5–0.6 mm	—	78.6 (78.6)	70

^{a} Total AVT of the material and the substrate (if any) under AM 1.5G and monthly max. spectra. The AVT under the cloudy avg. spectrum is marked in the bracket. AVTs across three spectra are nearly the same due to the insignificant difference in the spectral shape.

device's efficiency. One of the most commonly used encapsulants, EVA, is only capable of transmitting UV with wavelengths greater than 350 nm. Similar UV-opacity characteristics can also be observed in POE and PVB. Therefore, the selection of appropriate encapsulants is crucial in order to govern the PCE of the final STPV effectively.

In summary, the overall device performance of an STPV is significantly influenced by functional layers beyond the active absorber. Charge extraction layers, electrodes, and encapsulants play a crucial role in determining both the device's AVT and PCE. As a result, these components can substantially limit the achievable LUE of the entire device. Thus, to realize highly efficient and highly transparent STPVs, it is essential to enhance the transparency of these auxiliary layers across both the VIS and INVIS spectra.

4. Conclusions

Semi-transparent BIPVs hold great potential for green energy generation in urban environments. They offer seamless integration as windows and semi-transparent building envelopes, effectively leveraging existing building structures for solar energy harvesting without requiring additional space. Despite their appeal, there is a lack of quantitative data to accurately predict the maximum power generation of semi-transparent BIPVs in cities. These data rely on three crucial factors: (1) harvestable solar irradiance for STPVs in cities, (2) performance limits of different types of STPVs, and (3) the impact of different functional layers on the transparency and efficiency of STPVs. Access to such data is essential for informed optimization and performance prediction of semi-transparent BIPVs for urban applications.

To address this knowledge gap, we conducted an analysis of 10 years of solar irradiance data from 16 cities worldwide, considering various cloud cover conditions. Each dataset was categorized into three regions: ultraviolet (UV, 280–400 nm), visible (VIS, 400–700 nm), and shortwave infrared (IR, 700–3000 nm). Statistical analysis resulted in two empirical solar spectra: (I) monthly max., representing sunny conditions, and (II) cloudy avg., representing cloudy conditions. Additionally, we identified different STPV technologies, focusing on those achieved through the absorption modulation approach. Within this category, STPVs were further classified based on two VIS absorption methods: neutral density (ND) and band selective (BS), as well as three INVIS absorption modes: (i) UV, (ii) IR, and (iii) dual (UV + IR). This classification led to six absorption modulation strategies. We simulated the maximum performance parameters of these six strategies using both the standard AM 1.5G spectrum and the empirical solar spectra derived from our statistical analysis. While this work primarily utilizes examples of organic solar cells, the efficiency limits discussed are applicable to all STPV technologies. To evaluate the influence of charge extraction layers, electrodes, and encapsulants on overall device transparency and efficiency, we compiled the absorption spectra of common functional layers and calculated the AVT accordingly.

By comparing the six absorption modulation strategies in terms of their harvestable irradiance and performance limits in urban environments, and considering the influence of different functional layers, we have deduced the following findings:

(1) Harvestable solar irradiance for STPVs in cities

● The maximum solar irradiance values in cities reach 826 W/m^2 under realistic sunny skies and 95 W/m^2 under cloudy skies.

● In all 16 studied cities, IR constitutes approximately 50% of the total solar irradiance during sunny and mostly sunny conditions, which are prevalent (> 60% occurrence) weather patterns in most cities. Harnessing IR is crucial for efficient STPV systems.

● To maximize solar irradiance harvesting while maintaining high transparency, it is recommended to utilize IR or dual (UV + IR) absorption modes. In these modes, a completely transparent cell can achieve a harvestable irradiance of around 400 W/m^2 under clear skies and 40 W/m^2 under overcast skies, whereas the harvestable irradiance in UV mode is an order of magnitude lower.

(2) Performance limits of different types of STPVs

● For highly transparent devices with an absorber's AVT greater than 50%, the BS method is recommended due to its higher max. PCE, P_{out}, and LUE.

This journal is © The Royal Society of Chemistry 2025

Energy Environ. Sci., 2025, **18**, 579–601 | 597

• The {BS, UV, IR} combination consistently proves to be the most efficient strategy, with a PCE ranging from 14–33% depending on the desired AVT. It also achieves a maximum LUE of 20–23% for about 90% AVT. The resulting maximum P_{out} is greater than 150 W/m^2 under cloudless skies and 10–30 W/m^2 under overcast conditions. This strategy is also irradiance-tolerating at high AVT.

• Materials with bandgaps in the IR range (0.9–1.4 eV) are essential for achieving high-performance STPVs. They exhibit a max. PCE ranging from 14–33% across all three spectra (AM 1.5G, monthly max., and cloudy avg.) for both IR and dual (UV + IR) absorption modes.

• UV mode is applicable to both organic and inorganic materials, and the ideal bandgap falls within the range of 1.8–3.1 eV (VIS range).

(3) Impact of different functional layers on the transparency and efficiency of STPVs

• Metal electrodes typically have low transparency to both VIS and INVIS, which can attenuate device's AVT and PCE. However, this issue can be alleviated by either reducing the thickness to less than 10 nm or incorporating nanostructures.

• Most non-metal charge extraction layers and encapsulants possess high AVT values of 80–90%. However, some of these functional layers can block INVIS and potentially weaken the device's PCE.

In summary, the incorporation of IR absorption is vital for maximizing the utilization of total solar irradiance in STPVs. While the ND method allows for superior colour fidelity, the BS VIS absorption method offers greater efficiency for highly transparent STPVs. Organic materials with IR bandgaps enable the attainment of optimal efficiency while exhibiting high transparency to VIS in STPVs. When assessing the suitability of functional layers, it is important to consider their transparency to INVIS to ensure sustained performance levels.

Glossary

$\varphi^r(\lambda)$	Solar irradiance spectrum of AM 1.5G in spectral region r. Defined by eqn (1).
λ^r_{min}, λ^r_{max} (nm)	The minimum or maximum wavelength of the spectral region r.
λ^{VIS}_m (nm)	The central wavelength of VIS, defined to be $(400 + 700)/2 = 550$ nm.
$A^r_G(\lambda)$	Absorptance of the semi-transparent solar cell absorber in spectral region r that converts the solar irradiance spectrum to the harvestable irradiance spectrum for energy harvesting. The absorptance depends on the absorption strategy G.
Absorber AVT ($\Upsilon_{S;G}$)	The effective AVT of the absorber layer(s) in a semi-transparent solar cell. The brightness of the transmitted light only covers the visible region that is above the bandgap. Defined by eqn (6).
Absorption strategy G	The set of absorption characteristics in {...} consisting of the VIS absorption method and INVIS absorption mode. There are six possibilities in this study: {ND, UV}, {ND, IR}, {ND, UV, IR}, {BS, UV}, {BS, IR}, and {BS, UV, IR}.
AM 1.5G spectrum ($\Phi_0/(W\ m^{-2}\ nm^{-1})$)	Air Mass 1.5 global spectrum, a standard spectrum developed to represent the average terrestrial solar spectral irradiance over 48 contiguous U.S. states under a cloudless sky near noon.
AVT	Average visible transmittance: the brightness ratio of the transmitted VIS through a material related to the incident VIS perceived by human eyes.
BS	Band Selective: a visible light absorption modulation method for semi-transparent photovoltaics that selectively absorb specific wavelength bands of visible light while allowing others to transmit at full intensity. This method results in tinted transmission, with certain colours passing through at their original brightness while others are blocked. The wavelength interval to be absorbed depends on the absorption mode and desired average visible transmittance (AVT): UV: absorbs UV, then prioritizes absorption in the violet-end of visible spectrum. For high transparency, violet light is absorbed first, with absorption extending to longer wavelengths as AVT reduces. IR: absorbs IR, then prioritizes absorption in the red-end of the visible spectrum. For high transparency, red light is absorbed first, with absorption extending to shorter wavelengths as AVT reduces. UV + IR: absorbs UV and IR, then prioritizes absorption at both ends of the visible spectrum. For high transparency, violet and red light are absorbed first, with absorption extending from both ends towards green light as AVT reduces.
Device AVT	The AVT of the entire photovoltaic device, considering all its constituent layers.
E_g (eV)	Absorber bandgap.
$E_{g,opt}$ (eV)	PCE-optimal bandgap of the absorber. This absorber bandgap enables the Shockley–Queisser limit.
Harvestable irradiance (W/m^2)	The portion of solar irradiance available for a semi-transparent solar cell, depending on its absorption strategy for both visible and invisible lights.
Harvestable irradiance spectrum ($\tilde{\Phi}_{S;G}(\lambda)/(W\ m^{-2}\ nm^{-1})$)	Also spectral harvestable irradiance. The portion of solar irradiance spectrum available to a semi-transparent solar cell, determined by the irradiance condition S and absorption strategy G. Defined by eqn (3).
Harvesting VIS (α)	The fraction of brightness out of the visible light from the solar spectrum available to a semi-transparent solar cell for harvesting. Defined by eqn (4).
Irradiance condition S	Also the solar spectrum. Characterised by the local weather and climate. In this study, S is one of the three labels: 0 (as AM 1.5G), monthly max., and cloudy avg.
Cloudy avg. spectrum	An empirical solar spectrum derived from the AM 1.5G spectrum to represent the average terrestrial solar spectral irradiance over various latitudes across the globe under a cloudy sky (less than 20% clearness).
INVIS	Invisible light: radiations that are not detectable by the human eyes, collectively encompassing UV and IR.
INVIS absorption mode	The portion of invisible light targeted for power generation. Classified into three modes: UV: absorbs all UV and some visible light based on the desired transparency;

Table (*continued*)

	IR: absorbs all IR and some visible light based on the desired transparency; and dual (UV + IR): absorbs all UV and IR, and some visible light based on the desired transparency.
IR	Infrared radiation: invisible light with wavelengths longer than visible light (> 700 nm).
LUE	Light utilization efficiency: the product of AVT and PCE. Defined by eqn (5).
Monthly max. spectrum	An empirical solar spectrum derived from the AM 1.5G spectrum to represent the average terrestrial solar spectral irradiance over various latitudes across the globe under a sunny sky near noon.
ND	Neutral density: a visible light absorption modulation method for semi-transparent photovoltaics that uniformly attenuate a fraction of the visible light spectrum. This method aims to achieve a designated average visible transmittance (AVT) while maintaining colour neutrality. By absorbing incident visible light at an equal percentage across all wavelengths, the ND method preserves the relative spectral distribution of transmitted light, resulting in reduced brightness with minimal colour distortion.
P_{out} (W/m^2)	Output power intensity: the power intensity generated by the semi-transparent solar cell at the maximum power point.
PCE	Power conversion efficiency: the ratio of the output power intensity (P_{out}) to the solar irradiance (P_{in}).
Red-end VIS	The portion of the visible light spectrum with wavelengths approaching the IR region, typically around 650–700 nm.
Solar irradiance (P_{in}/(W/m^2))	The wavelength-integrated solar radiation per unit area reaching a specific surface on Earth, which is the input power for calculating the PCE of a solar cell.
Solar irradiance spectrum ($\Phi_S(\lambda)$/(W m^{-2} nm^{-1}))	Also spectral solar irradiance. The spectral irradiance of solar radiation reaching a specific surface on Earth. Depends on the irradiance condition S. Defined by eqn (2).
Spectral region r	Label of spectral range of an irradiance spectrum. r = UV, VIS, and IR.
SQ limit	Shockley–Queisser limit: the theoretical maximum possible PCE achieved by a solar cell of voltage corresponding to its bandgap. The efficiency is limited by subgap loss, thermal relaxation, detailed balance and fill factor.
UV	Ultraviolet radiation: invisible light with wavelengths shorter than visible light (280–400 nm).
$V(\lambda)$	Luminous efficiency function: the human eye sensitivity for different visible wavelengths.
Violet-end VIS	The portion of the visible light spectrum with wavelengths approaching the UV region, typically around 400–450 nm.
VIS	Visible light: the portion of the solar spectrum that is detectable by the human eye, with wavelengths ranging between 400–700 nm.
VIS absorption method	Methods for modulating the absorption of visible light in semi-transparent solar cells. Classified into neutral density (ND) and band selective (BS) methods.
w_S^r	Weighting factor or relative intensity of spectrum S in spectral region r compared to AM 1.5G. The value can be greater than or less than unity.

Data availability

This study was carried out using publicly available solar irradiance data from NASA at https://power.larc.nasa.gov/data-access-viewer/.

Conflicts of interest

There are no conflicts of interest to declare.

Acknowledgements

References

1 IEA, *Tracking Clean Energy Progress*, IEA Paris, France, 2023.
2 A. K. Shukla, K. Sudhakar and P. Baredar, *Energy Build.*, 2017, **140**, 188–195.
3 E. Biyik, M. Araz, A. Hepbasli, M. Shahrestani, R. Yao, L. Shao, E. Essah, A. C. Oliveira, T. Del Cano and E. Rico, *Eng. Sci. Technol. Int. J.*, 2017, **20**, 833–858.
4 T. E. Kuhn, C. Erban, M. Heinrich, J. Eisenlohr, F. Ensslen and D. H. Neuhaus, *Energy Build.*, 2021, **231**, 110381.
5 M. Saifullah, J. Gwak and J. H. Yun, *J. Mater. Chem. A*, 2016, **4**, 8512–8540.
6 P. Kumar, S. You and A. Vomiero, *Adv. Energy Mater.*, 2023, **13**, 2301555.
7 M. M. Tavakoli, R. Po, G. Bianchi, A. Cominetti, C. Carbonera, N. Camaioni, F. Tinti and J. Kong, *Proc. Natl. Acad. Sci. U. S. A.*, 2019, **116**, 22037–22043.
8 J. Jing, S. Dong, K. Zhang, Z. Zhou, Q. Xue, Y. Song, Z. Du, M. Ren and F. Huang, *Adv. Energy Mater.*, 2022, **12**, 2200453.
9 Y. Xie, L. Huo, B. Fan, H. Fu, Y. Cai, L. Zhang, Z. Li, Y. Wang, W. Ma and Y. Chen, *Adv. Funct. Mater.*, 2018, **28**, 1800627.
10 N. C. Davy, M. Sezen-Edmonds, J. Gao, X. Lin, A. Liu, N. Yao, A. Kahn and Y.-L. Loo, *Nat. Energy*, 2017, **2**, 1–11.
11 T. Jiang, G. Zhang, R. Xia, J. Huang, X. Li, M. Wang, H.-L. Yip and Y. Cao, *Mater. Today Energy*, 2021, **21**, 100807.
12 C.-C. Chen, L. Dou, J. Gao, W.-H. Chang, G. Li and Y. Yang, *Energy Environ. Sci.*, 2013, **6**, 2714–2720.
13 G. E. Eperon, D. Bryant, J. Troughton, S. D. Stranks, M. B. Johnston, T. Watson, D. A. Worsley and H. J. Snaith, *J. Phys. Chem. Lett.*, 2015, **6**, 129–138.

This journal is © The Royal Society of Chemistry 2025

Energy Environ. Sci., 2025, **18**, 579–601 | **599**

14 J. Yoon, A. J. Baca, S.-I. Park, P. Elvikis, J. B. Geddes III, L. Li, R. H. Kim, J. Xiao, S. Wang and T.-H. Kim, *Nat. Mater.*, 2008, **7**, 907–915.

15 M. G. Debije and P. P. Verbunt, *Adv. Energy Mater.*, 2012, **2**, 12–35.

16 B. Zhang, C. Gao, H. Soleimaninejad, J. M. White, T. A. Smith, D. J. Jones, K. P. Ghiggino and W. W. Wong, *Chem. Mater.*, 2019, **31**, 3001–3008.

17 D. Kim, S. S. Shin, S. M. Lee, J. S. Cho, J. H. Yun, H. S. Lee and J. H. Park, *Adv. Funct. Mater.*, 2020, **30**, 2001775.

18 J. H. Heo, H. J. Han, M. Lee, M. Song, D. H. Kim and S. H. Im, *Energy Environ. Sci.*, 2015, **8**, 2922–2927.

19 K. Lee, N. Kim, K. Kim, H.-D. Um, W. Jin, D. Choi, J. Park, K. J. Park, S. Lee and K. Seo, *Joule*, 2020, **4**, 235–246.

20 B. Zhang, P. Zhao, L. J. Wilson, J. Subbiah, H. Yang, P. Mulvaney, D. J. Jones, K. P. Ghiggino and W. W. Wong, *ACS Energy Lett.*, 2019, **4**, 1839–1844.

21 C. Momblona, O. Malinkiewicz, C. Roldán-Carmona, A. Soriano, L. Gil-Escrig, E. Bandiello, M. Scheepers, E. Edri and H. Bolink, *APL Mater.*, 2014, **2**, 081504.

22 Z. Zhang, R. Ji, X. Jia, S. J. Wang, M. Deconinck, E. Siliavka and Y. Vaynzof, *Adv. Funct. Mater.*, 2023, 2307471, DOI: **10.1002/adfm.202307471**.

23 F. Bernal-Texca, E. Andrioti, J. Martorell and C. Ros, *Energy Environ. Mater.*, 2024, e12809, DOI: **10.1002/eem2.12809**.

24 J. Goffard, A. Cattoni, F. Mollica, M. Jubault, C. Colin, J.-F. Guillemoles, D. Lincot, N. Naghavi and S. Collin, presented in part at the EU PVSEC, 2015.

25 R. R. Lunt, *Appl. Phys. Lett.*, 2012, **101**, 043902.

26 C. J. Traverse, R. Pandey, M. C. Barr and R. R. Lunt, *Nat. Energy*, 2017, **2**, 849–860.

27 N. Yao, Y. Xia, Y. Liu, S. Chen, M. P. Jonsson and F. Zhang, *ACS Appl. Energy Mater.*, 2021, **4**, 14335–14341.

28 Z. Hu, Z. Wang and F. Zhang, *J. Mater. Chem. A*, 2019, 7, 7025–7032.

29 C. Xu, K. Jin, Z. Xiao, Z. Zhao, Y. Yan, X. Zhu, X. Li, Z. Zhou, S. Y. Jeong and L. Ding, *Solar RRL*, 2022, **6**, 2200308.

30 D. Luo, Y. Zhang, L. Li, C. Shan, Q. Liu, Z. Wang, W. C. Choy and A. K. K. Kyaw, *Mater. Today Energy*, 2022, **24**, 100938.

31 F. Matteocci, D. Rossi, L. A. Castriotta, D. Ory, S. Mejaouri, M. A. der Maur, F. Sauvage, S. Cacovich and A. Di Carlo, *Nano Energy*, 2022, **101**, 107560.

32 J. H. Noh, S. H. Im, J. H. Heo, T. N. Mandal and S. I. Seok, *Nano Lett.*, 2013, **13**, 1764–1769.

33 L. Yuan, Z. Wang, R. Duan, P. Huang, K. Zhang, Q. Chen, N. K. Allam, Y. Zhou, B. Song and Y. Li, *J. Mater. Chem. A*, 2018, **6**, 19696–19702.

34 J. Barichello, D. Di Girolamo, E. Nonni, B. Paci, A. Generosi, M. Kim, A. Levtchenko, S. Cacovich, A. Di Carlo and F. Matteocci, *Solar RRL*, 2023, **7**, 2200739.

35 L. Zuo, X. Shi, W. Fu and A. K. Y. Jen, *Adv. Mater.*, 2019, **31**, 1901683.

36 Y. Li, X. Huang, H. K. Sheriff Jr and S. R. Forrest, *Nat. Rev. Mater.*, 2023, **8**, 186–201.

37 G. P. Kini, S. J. Jeon and D. K. Moon, *Adv. Funct. Mater.*, 2021, **31**, 2007931.

38 Z. Hu, J. Wang, X. Ma, J. Gao, C. Xu, K. Yang, Z. Wang, J. Zhang and F. Zhang, *Nano Energy*, 2020, **78**, 105376.

39 K. Khandelwal, S. Biswas, A. Mishra and G. D. Sharma, *J. Mater. Chem. C*, 2022, **10**, 13–43.

40 R. Gui, K. Xian, Y. Shi, W. Zhang, J. Qiao, Z. Fu, J. Wang, F. Cui, Q. Wang and V. K. Wong, *Adv. Energy Mater.*, 2023, **13**, 2302029.

41 T. Liu, Q. C. Burlingame, J. C. Sorli, M. L. Ball, G. Cheng, N. Yao and Y. L. Loo, *Adv. Energy Mater.*, 2021, **11**, 2100225.

42 V. K. Wong, C. Zhang, Z. Zhang, M. Hao, Y. Zhou and S. K. So, *Mater. Today Energy*, 2023, 101347, DOI: **10.1016/j.mtener.2023.101347**.

43 B. A. Wielicki, B. R. Barkstrom, E. F. Harrison, R. B. Lee III, G. L. Smith and J. E. Cooper, *Bull. Am. Meteorol. Soc.*, 1996, **77**, 853–868.

44 B. A. Wielicki, B. R. Barkstrom, B. A. Baum, T. P. Charlock, R. N. Green, D. P. Kratz, R. B. Lee, P. Minnis, G. L. Smith and T. Wong, *IEEE Trans. Geosci. Remote Sens.*, 1998, **36**, 1127–1141.

45 CERES SYN1deg-1Hour Terra-Aqua Edition4A, **https://doi.org/10.5067/TERRA+AQUA/CERES/SYN1DEG-1HOUR_L3.004A**, (accessed December 2023).

46 J. Randall and J. Jacot, *Renewable Energy*, 2003, **28**, 1851–1864.

47 Reference Air Mass 1.5 Spectra, **https://www.nrel.gov/grid/solar-resource/spectra-am1.5.html**, (accessed 01 December, 2022).

48 J. H. Seinfeld and S. N. Pandis, *Atmospheric chemistry and physics: from air pollution to climate change*, John Wiley & Sons, 2016.

49 J. K. W. Ho, H. Yin and S. K. So, *J. Mater. Chem. A*, 2020, **8**, 1717–1723.

50 H. Yin, J. K. W. Ho, V. Piradi, S. Chen, X. Zhu and S. K. So, *Small Methods*, 2020, **4**, 2000136.

51 W. Shockley and H. Queisser, *Appl. Phys.*, 1961, **32**, 510–519.

52 O. D. Miller, E. Yablonovitch and S. R. Kurtz, *arXiv*, 2011, preprint, arXiv:1106.1603, DOI: **10.48550/arXiv.1106.1603**.

53 D. Yang, X. Zhang, X. Huang, L. Shen, J. Huang, X. Chang and G. Xing, MobiCom '20: Proceedings of the 26th Annual International Conference on Mobile Computing and Networking, London, United Kingdom, September, 2020.

54 K.-T. Lee, L. J. Guo and H. J. Park, *Molecules*, 2016, **21**, 475.

55 Y. Xu, J. Wang, L. Sun, H. Huang, J. Han, H. Huang, L. Zhai and C. Zou, *J. Mater. Chem. C*, 2021, **9**, 9102–9123.

56 E. Hecht, *Optics*, Pearson Education, India, 5th edn, 2002.

57 W. Ke, D. Zhao, A. J. Cimaroli, C. R. Grice, P. Qin, Q. Liu, L. Xiong, Y. Yan and G. Fang, *J. Mater. Chem. A*, 2015, **3**, 24163–24168.

58 T. Xu, B. Deng, Y. Zhao, Z. Wang, G. Lévêque, Y. Lambert, B. Grandidier, S. Wang and F. Zhu, *Adv. Energy Mater.*, 2023, **13**, 2301367.

59 T. Xu, Y. Luo, S. Wu, B. Deng, S. Chen, Y. Zhong, S. Wang, G. Lévêque, R. Bachelot and F. Zhu, *Adv. Sci.*, 2022, **9**, 2202150.

60 J. Sun, N. Zhang, J. Wu, W. Yang, H. He, M. Huang, Y. Zeng, X. Yang, Z. Ying and G. Qin, *ACS Appl. Mater. Interfaces*, 2022, **14**, 52223–52232.

61 W.-F. Chen, P. Koshy and C. C. Sorrell, *J. Mater. Sci.*, 2016, **51**, 2465–2480.

600 | *Energy Environ. Sci.*, 2025, **18**, 579–601

This journal is © The Royal Society of Chemistry 2025

62 J. Li, J. Yao, H. Xia, W. Sun, J. Liu and L. Peng, *Appl. Phys. Lett.*, 2015, **107**, 013901.

63 Z. Liu, J. Li, Z.-H. Sun, G. Tai, S.-P. Lau and F. Yan, *ACS Nano*, 2012, **6**, 810–818.

64 S. B. Shivarudraiah, N. Tewari, M. Ng, C.-H. A. Li, D. Chen and J. E. Halpert, *ACS Appl. Mater. Interfaces*, 2021, **13**, 37223–37230.

65 J. Gong, R. Dai, Z. Wang and Z. Zhang, *Sci. Rep.*, 2015, **5**, 9279.

66 P. Patoka and M. Giersig, *J. Mater. Chem.*, 2011, **21**, 16783–16796.

67 M. Z. Burrows, A. Meisel, F. Lemmi, H. Antoniadis, S. Schreiber, L. Garreau-Iles, P. Boydell, A. M. Bennett and R. L. Smith, 2012 38th IEEE Photovoltaic Specialists Conference, Austin, Texas, USA, June, 2012.

68 S. Ohl and G. Hahn, 23rd European Photovoltaic Solar Energy Conference, Valencia, Spain, September, 2008.

69 R. Heidrich, C. Barretta, A. Mordvinkin, G. Pinter, G. Oreski and R. Gottschalg, *Sol. Energy Mater. Sol. Cells*, 2024, **266**, 112674.

70 C. Piwnuan, J. Wootthikanokkhan and C. Muangphat, *J. Mater. Chem. C*, 2023, **11**, 13946–13956.

This journal is © The Royal Society of Chemistry 2025

Energy Environ. Sci., 2025, **18**, 579–601 | **601**